Bachelor Thesis:

STUDY ON NUMERICAL DIFFUSION IN ALIGNED AND NON-ALIGNED MESHES FOR MAGNETICALLY CONFINED PLASMA TRANSPORT EQUATIONS

Author: Óscar González Martínez
Tutor: Daniel Pérez Grande

Bachelor's Degree in Aerospace Engineering

Leganés, June 2015

Abstract

One of the main challenges present in the numerical modeling of magnetically confined plasmas is due to the highly anisotropic nature of these systems. In certain electric propulsion engines, such as electromagnetic thrusters, plasma discharges occur under complex magnetic field configurations, which requires the use of appropriate computational meshes to precisely simulate the behaviour of the plasma and obtain the least numerical error.

This Bachelor Thesis is devoted to estimating the numerical error induced when posing the anisotropic plasma diffusion equation in structured, unaligned meshes, in order to address the benefits derived from the use of Magnetic Field-Aligned Meshes (MFAMs) in highly anisotropic problems. It is discussed whether typical discretization errors due to gradient reconstruction methods and low quality mesh elements in MFAMs are comparable to those induced by numerical diffusion in unaligned meshes.

First, the evolution of a highly anisotropic system in a computational mesh unaligned with the magnetic field is analyzed. By means of an average error, numerical diffusion will be quantified attending to different parameters: mesh refinement, magnetic field misalignment, geometric mesh quality, and various anisotropicity levels. Furthermore, a qualitative analysis is performed to show how these factors contribute to numerical diffusion.

Then, a benchmark comparison of the evolution of a highly anisotropic problem in a strcutured, non-aligned mesh against the solution in a MFAM is provided. Additionally, errors due to gradient reconstruction in the non-structured MFA mesh are discussed.

It is concluded that, in spite of the errors that may arise due to gradient reconstruction methods or low geometric mesh quality regions, Magnetic Field-Aligned Meshes provide with a more correct approach in the modeling of highly anisotropic systems, specially if the anisotropicity level is not known a-priori.

Contents

List of Figures

Chapter 1

Introduction

1.1 Motivation

Humanity's interest in stepping into outer space has fostered an unparalleled technological development over the past decades. The desire to explore and push the boundaries of our knowledge has served to overcome the scientific and technical challenges of space exploration. Humans' wish of going deeper into space has triggered a continuous development, from the first satellites in orbit to the space probes that are actually beyond the boundaries of the solar system.

Part of this development has been focused on the improvement of spacecraft propulsion systems. Among them, electric propulsion (EP) is seen as an attractive alternative to conventional propulsion systems (i.e.: chemical propulsion, CP). Furthermore, as part of these advances, numerical simulations are routinely used in the development of engines with better performances, in the quest for a new generation of EP thrusters. Enormous efforts are being done in terms of development of accurate models, to precisely simulate the behaviour of the ionized propellant being expelled by the engines, and the performances that may be derived from the intimate knowledge of such behaviour. The main reason is that the development costs and timescales for these engines (which include both the engines themselves and the experimental facilities required for their testing) are, respectively, high and lengthy; the development of accurate simulation codes is attractive in order to aid the development process and reduce costs.

An important problem arising in numerical simulations of certain EP systems such as electromagnetic thrusters (those in which the engine operation relies on electromagnetic forces) is due to the highly anisotropic nature of a magnetized plasma, as it induces an undesirable error when solving the transport equations if the computational grid is unaligned with the magnetic field. This issue, which will be discussed in this project, conditions the type of mesh used in numerical

simulation if we wish to obtain the least numerical error. Specifically, the anisotropic plasma diffusion equation can be posed in not-aligned meshes with the magnetic field and in Magnetic Field Aligned (MFA) meshes.

Not-aligned meshes offer a simpler approach on the modeling of plasma thrusters compared to MFA meshes, mainly due to the fact that building of such models is relatively simple and, in general, allows for an easier implementation of the algorithm to solve the equations. However, these meshes present an intrinsic numerical error due to the element facets not being aligned with the magnetic field, as will be shown in Chapter 2. On the other hand, the inherent benefits of a MFA mesh, even in a highly anisotropic medium, are that the induced numerical error will not be present since, in these type of meshes, the element facets are locally aligned with the magnetic field lines. Nonetheless, MFA meshes are more expensive to build and usually require a more robust gradient reconstruction method than, for instance, structured, not-aligned meshes.

As part of the work developed by the EP2 group at UC3M, and by means of an advanced platform currently under development used to generate the MFA mesh with the desired magnetic field topology (NOMADS - NOn-Structured Magnetically Aligned plasma Discharge Simulation-), this project aims to give an insight on the order of the error induced when solving the plasma transport equation using Magnetic Field Aligned versus non-aligned meshes; which currently stands as an existing discussion in the space propulsion community.

1.2 Electric Propulsion systems

An electric propulsion system gathers any propulsion technology that aims at achieving thrust, by means of generation and further acceleration of a plasma (the ionized state of the propellant) up to very high exhaust velocities, using electricity.

An electric thruster requires less amount of propellant for a given thrust than, for instance, chemical engines, which confers them a greater autonomy for a given mission. On the contrary, in spite of having a higher exhaust velocities, electric thrusters work with much smaller flows, resulting in thrust of some fraction of a Newton [6]. The reason behind this is that, while chemical propulsion engines are energy-limited by the chemical energy stored within the propellant, an EP system is power-limited by the available power inside a spacecraft. Nonetheless, development of solar-electric and nuclear-electric power plants for spacecraft is driving research on EP thrusters with even increasing electrical power.

The direct consequence of having such low thrust values is the long transfer times when performing significant orbit changes. In addition, the erosion of the wall boundaries due to high-energy ion collision, a phenomenon also known as

sputtering, drastically reduces the lifetime of such thrusters. This represents a shortcoming and can limit their applicability on long missions, which is somehow exacerbated due to the fact that the experimental characterization of this erosion, needed to be carried out to certify thruster lifetimes, represents large timescales and high testing costs. Therefore, while testing will undoubtedly be required for certification efforts, the use of numerical simulations offers insight into how particular designs will perform and may open previously unknown optimization opportunities.

Nowadays, the widespread scope of application of electric propulsion systems includes geosynchronous communication satellites, orbit insertion and deep-space missions; as an acceptance of the maturity stage of this technology. In fact, the enormous advantages previously discussed lead to immense cost savings if electric propulsion is used. To give an example, according to [7] and [8] assuming a cost of $30,000 to launch 1 Kg of payload to a Geostationary Orbit (GEO), mission cost savings can account for more than $20 million if the spacecraft is powered using electric means.

Moreover, current research seeks to improve already developed EP technologies to broaden their scope to deep space missions, achieving cost savings by substituting today's used electric propulsion engines; despite presumably assuming a non-recurring investment. On this line, NASA is willing to improve Hall Effect thruster technology to compete with the nowadays used Gridded Ion thruster in Dawn mission. Mission recurring costs are assumed to be reduced by one order of magnitude [9].

Among the different categories of EP systems, it is of interest to focus on electromagnetic thrusters, in which electric and magnetic fields are generated to accelerate highly ionized plasmas. In these devices a magnetic field is responsible for electron confinement. Thus, leading to the highly anisotropic nature of the magnetized plasma we wish to study; the lack of prior knowledge of the degree of anisotropicity in the magnetized plasma points to the use of MFA meshes, against not-aligned meshes in order to avoid the aforementioned induced error.

1.2.1 Electromagnetic thrusters

In general, an electromagnetic device is characterized by the use of different magnetic topologies designed for electron confinement and/or acceleration of the plasma. The operation of these engines is based on the acceleration of the charged propellant by the Lorentz forces generated by an electromagnetic field. In the presence of an electric field $\vec{E}$ and magnetic field $\vec{B}$ the reaction of a particle, with charge q and velocity $\vec{v}$, will be given by the Lorentz force:

$$\vec{F_L} = m\frac{d\vec{v}}{dt} = q(\vec{E} + \vec{v} \times \vec{B}) \tag{1.1}$$

Being its associated gyroradius or Larmor radius given by:

$$r_g = \frac{mv_\perp}{qB} \tag{1.2}$$

Because of typically low intensity magnetic fields, lighter particles such as electrons have a Larmor radius much smaller than the characteristic length of the thruster and thus, will be more likely to be "magnetized" (confined by the magnetic field) than heavier species (i.e.: ions). In addition, the propellant exhaust velocities will lie on the strength of the electromagnetic field and temperature of the plasma. In engines such as Hall Effect thrusters, the exhaust velocity is directly related to the strength of the electric field. The coupling of the reaction forces to the propellant is typically done in the magnetic circuit.

The classification of the different electromagnetic devices can be done attending to the different magnetic field configurations and the mechanism employed for the acceleration the ionized propellant; two main groups are of interest to us:

1. Devices in which ion acceleration is established by an external magnetic or electric field, such as Hall Effect thrusters (HET) and its variants with magnetic cusps: Diverging Cusped Field thrusters (DCFT) and High Efficient Multistage Plasma Thrusters (HEMPT), and Magnetoplasmadynamic Thrusters (MPDT).

2. Devices in which plasma is first heated and then expanded on magnetic nozzles. This encompasses different EP thrusters with magnetic nozzle: Electron-Cyclotron Resonance (ECR), Helicon Plasma Thrusters (HPT), and Variable Specific Impulse Magnetoplasma Rocket (VASIMR).

Both groups will be discussed in more detail in succeeding paragraphs.

External electric or magnetic field for ion acceleration

In these engines, confinement of the electron population from the chamber walls is attained by an external magnetic field, restricting the motion of electrons to the anode and enhancing impacts with the atoms of the propellant. Several technologies based on this principle are:

- Hall Effect Thrusters

Hall Effect thrusters offer a much simpler configuration in terms of design and power supply compared to other types of EP systems. Plasma is produced by means of a cross-field discharge channel formed by an axial electric field and a radial magnetic field. Electrons are expelled through a cathode located in the exterior part of the nozzle. Some of them enter the thruster due to the presence of the electric field and get confined, describing a spiral pattern along the generated radial magnetic field lines inside the channel due to the $\overrightarrow{E} \times \overrightarrow{B}$ drift; while others neutralize the charged exhaust stream (see Figure 1.1).

The propellant is fed into the thruster through an injector, and becomes ionized due to the collisions with the confined electrons. Forced by these collisions and plasma instabilities, some electrons will thereby diffuse and close the electric circuit by moving toward the anode, located close to the injector. While the ions will be expelled following the axial electric field with very high exhaust velocities through the nozzle, leading to a I_{sp} in the range of $15-30Kms^{-1}$. Notwithstanding, HETs may lead to lower thruster efficiencies compared to other types of EP systems; for instance, for the same input power, the efficiency of a HET will be 15% lower than for an Ion thruster device [5].

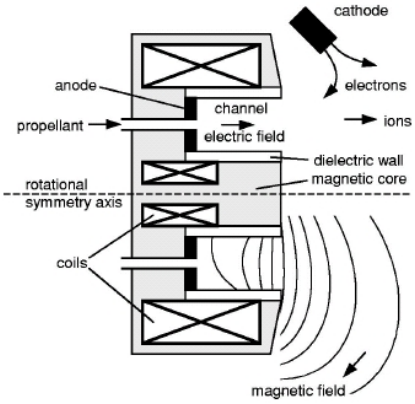

Figure 1.1: Schematic of a Hall-Effect thruster. Source: Laplace university, France

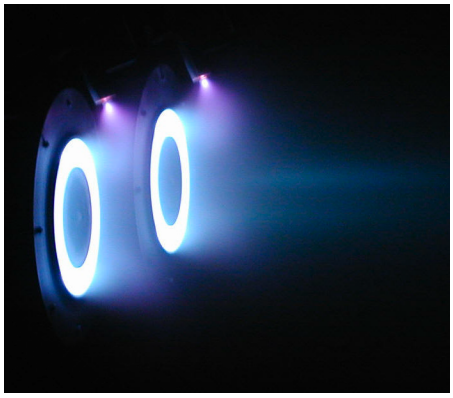

Figure 1.2: Testing of two Hall-Effect thrusters. Source: Alta-Space

Although HETs admit several types of propellants in which krypton and argon are included, xenon is sometimes the preferred option, and this is because of the offered important characteristics that are not present in other propellant candidates. Xenon is not a hazardous substance, thus, allowing safe handling and processing. In addition, its higher mass results in larger thrust for the same input power. However, there are also detrimental features that preclude its use in high power thrusters, namely the high cost incurred when utilized in long missions, and ground testing difficulties [10].

Two different versions providing different capabilities might be distinguished in the field of Hall Effect Thrusters: Stationary Plasma Thruster (SPT), offering a larger acceleration channel that requires the use of ceramic materials to protect the walls since erosion is enhanced due to the continuous bombardment of electrons. The second version is the Thruster with Anode Layer (TAL), whose walls are made of metallic materials. The combination of different geometries, as well as materials, strongly affects the underlying physics of both models. An example of a Magnetic Field-Aligned Mesh for the SPT-100 magnetic configuration is presented in Figure 1.3

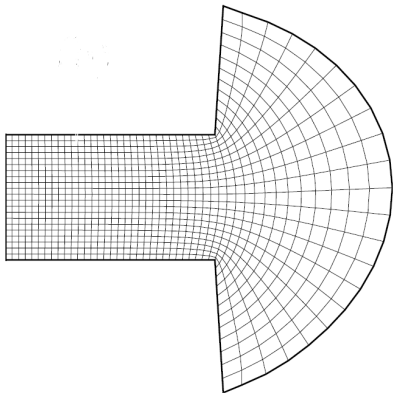

Figure 1.3: MFAM for the SPT-100 magnetic topology (axisymmetric simulation domain). Source: Ref. [1]

The most renowned application of a Hall-Effect Thruster (HET) was its use in 2003 for the European Space Agency (ESA) lunar mission: SMART-1. Conventionally, they present an annular geometry, although the design of cylindrical Hall-Effect thrusters is becoming more popular since it allows to be readily scaled to smaller sizes.

- High Efficient Multistage Plasma Thrusters and Diverging Cusped Field Thrusters

The problems arising from a typical HET related to wall erosion and plasma losses may be eluded by the considerably recent DCFT and HEMPT. Both introduce an innovative cusped magnetic topology that enhances electron confinement at the chamber walls and shields the inner wall from sputtering, despite the operating principle being identical to that of HETs. As depicted in Figure 1.4, the configuration aims to generate parallel lines to the inner annular walls for most of the discharge channel, seldom intersecting with the wall boundaries (i.e.: at the magnetic cusps). It is in the innermost cusped regions, in which $\vec{B}$ is mostly radial, where most of the electrons are expected to be confined by $\vec{E} \times \vec{B}$ effects, and where diffusion due to impacts with the atoms of the gas will ensure the required current for the engine operation [2].

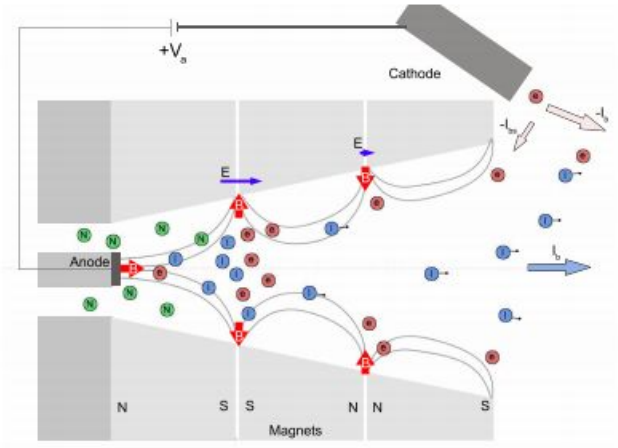

Figure 1.4: Magnetic field topology in a DCFT. Source: Ref. [2]

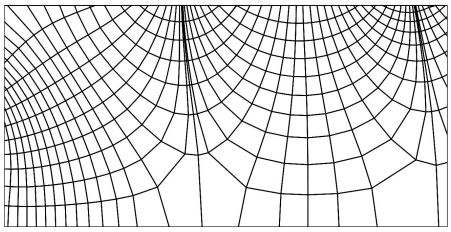

Figure 1.5: MFAM for a cusped magnetic field (axisymmetric simulation domain). Source: Ref. [3]

In a HEMPT, the specific cusped magnetic field configuration provided by a sequential arrangement of permanent magnets guarantees that the plasma fluxes to the walls can only occur at the magnetic cusps. This magnetic topology also serves as an impediment for electron motion toward the anode. Additionally, ions are accelerated in a more efficient manner since the cusped configuration allows for the formation of large electric field gradients [11].

Specifically, the DCFT can be considered to be an improved version of a HEMP [2]. As shown in Figure 1.4, what are called "magnetic bottles", appear near the anode and at the cusps, which favours the large magnetic and electric gradients required for electron confinement and ion acceleration. It is worth to mention that the last magnetic cusp at the engine exit is not only intended to provide a further region of confinement, but to create a configuration similar to that of a magnetic nozzle, ultimately expanding the ionized propellant.

- Magnetoplasmadynamic Thruster

A competitive propulsion candidate for high power missions may be represented by MPD thrusters. Essentially, a MPD thruster is a simple device that consists on

a central cathode and a partially divergent coaxial anode ring, in between which a voltage is generated (in the range 50-300V [5]). The ionization of the propellant leads to a longitudinal plasma current that generates an azimuthal magnetic field. The acceleration of the charged particles is due to the Lorentz force, resulting in potentially high thrust, up to $25N$, with a specific impulse close to $8,000s$, being their main drawback the enormous power requirements [8] [4].

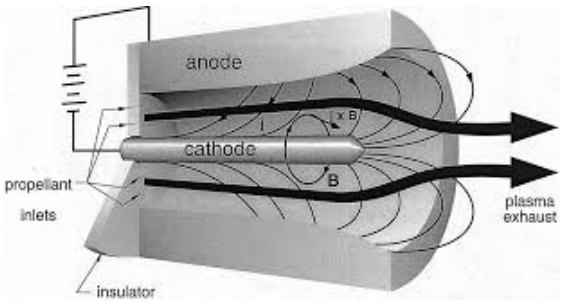

Figure 1.6: Magnetic field topology in a MPD. Source: Ref.[4]

Thrusters with Magnetic Nozzle

This second type of engines requires the use of a magnetic nozzle (MN) to convert the thermal energy of a highly ionized plasma into kinetic energy. A MN employs an axisymmetric convergent-divergent magnetic field generated by a set of permanent magnets or electromagnetic coils, which provides plasma confinement apart from accelerating and guiding the plasma beam into vacuum. The use of coils allows to tweak the configuration of the magnetic field and adjust it to attain better performances according to the system needs, increasing the versatility of these thrusters.

A distinct advantage of MNs is the prevented interaction between plasma and thruster walls, which promotes the use of these devices as an alternative to other types of thrusters. Notwithstanding, the absence of solid walls requires a sufficiently robust magnetic field to effectively control the expansion of the supersonic plasma jet.

- Electron-Cyclotron Thruster

There are several technologies that benefit from having a MN. For instance, in an Electron-Cyclotron Resonance thruster (see Figure 1.7) ionization of the gas is achieved by applying a micro-wave electromagnetic field at the same frequency at which electrons gyrate around the field lines (resonance frequency). This results in an ionization of the propellant that stems from efficiently heating the electrons up to very high temperatures. The acceleration of the charged species occurs at the magnetic nozzle, where the ambipolar electric field produced by the electrons

exiting the thruster accelerates the weakly magnetized ions downstream, ensuring space charge neutrality of the plasma beam.

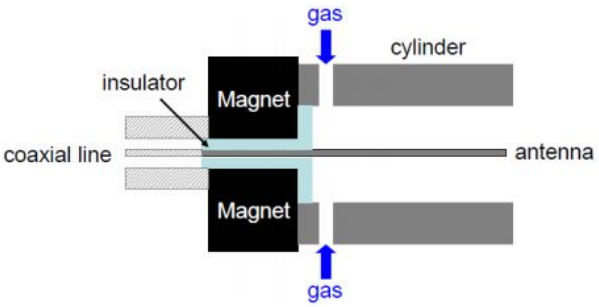

Figure 1.7: Schematic of an ECR thruster. Source: Ref.[2]

- Helicon Plasma Trhusters

In the scope of thrusters with magnetic nozzle, the Helicon Plasma Thruster (HPT) is a promising advanced propulsion alternative and somewhat similar to the ECR thruster, although existent prototypes have demonstrated to have low efficiencies (close to 20%) [12]. The undergoing tests of HPT feature an efficient use of radio frequencies (RF) to produce plasma at high temperatures.

As shown in Figure 1.8, the thruster design consists on a cylindrical vessel, in which a set of solenoids are used to generate a quasi-axial magnetic field. A RF antenna wound around the dielectric tube is used to ionize the propellant. The strength of the magnetic field can vary up to thousands of Gauss, while the emitting frequency of the antenna usually ranges between 1 to 25 MHz [5]. The remaining deposited energy on the electrons once the propellant is energized is used to accelerate both species in the magnetic nozzle by means of the established ambipolar electric field.

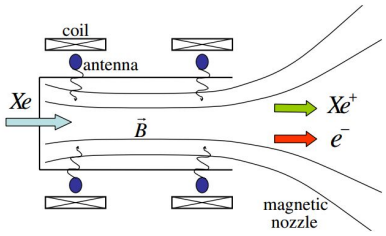

Figure 1.8: Schematic of a HPT. Source: Ref.[5]

What really differentiates Helicon thrusters from other technologies is the larger plasma density it is able to handle (up to $10^{20}m^{-3}$), leading to $I_{sp} > 1,200s$ with a thrust of 1.5 mN [13]

- Variable Specific Impulse Magnetoplasma Rocket

The VASIMR can be seen as an improved version of a HPT in terms of power. It consists on the two stages present in a HPT (RF ionization and magnetic nozzle) with an Ion Cyclotron Resonance (ICR) antenna as the principal heating stage in between the two (see Figure 1.9). This added phase is aimed to deposit energy in ions, which results in a highly anisotropic ion population (as opposed to HPT, where the ambipolar electric field was driven by the electrons). In addition, and as it can be inferred form its name, these devices allow to adjust their I_{sp} and thrust by modifying their mas flow, ICR power and magnetic nozzle.

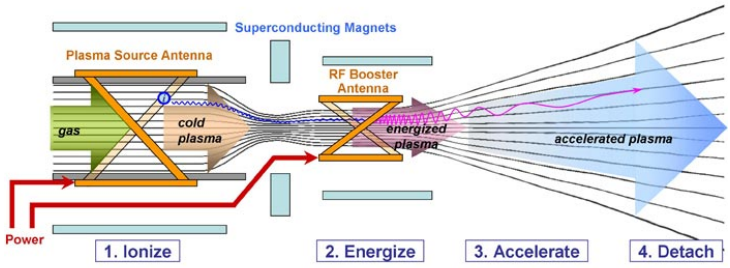

Figure 1.9: Schematic of a VASIMR. Source: Ad Astra Rocket

Among several concerns, the most outstanding is the strength of the magnetic field required to magnetize the ions, which needs to be larger than 2 Teslas to favour ion confinement. This is sidestepped by introducing high-temperature superconductors, assuming the consequent mass increment. All in all, the operation of the thruster with all the stages active has demonstrated a much higher efficiency than HPT ($\sim 70\%$) with a thrust of 6N and a $I_{sp} = 50km/s$[14].

1.2.2 Impact of simulation codes on future developments

It is worth mentioning that an essential feature present in future technological advances is constituted by the development of numerical models, even more accurate that today's tools, allowing to simulate a wide variety of magnetic field topologies without the need of incurring in high testing costs.

Future improvements are aligned with the development of these simulation tools. For instance, the MIT research laboratory is extending the possibilities regarding already developed codes for the modeling of Hall-Effect thrusters, together with the use of a real HET as a benchmark to validate these codes [15]. Parallel work related to the development of higher-efficiency and improved capabilities EP engines is also being done at the California Institute of Technology, at the Jet Propulsion Laboratory facilities.

In addition, successful efforts are also being made in Europe, where several research teams are established devoted to the study of the underlying physics involved in the generation and further acceleration of plasma. For instance, the mentioned EP2 group at UC3M drives part of its research on the numerical modeling of the engine operation, studying the effect of the different parameters on the performances to allow for future design and modifications of the different types of plasma thrusters. This is done through implementation and development of advanced platforms such as HP-HALL2, HallMA, and NOMADS.

Moreover, the European Space Agency has incorporated EP systems in unmanned spacecraft missions. And what is more, specific programs to enable major advances in EP, trying to guarantee a much more competitive development are being launched in regards of the Horizon 2020 [16].

1.3 Project objectives

The effect of the magnetic field topology in the EP thrusters mentioned is crucial, as it may allow for the reduction of erosion if, for example, field lines remain parallel to the wall. It might also be used to enhance plasma confinement and, therefore, increase beam control, being able to "focus" the expelled ion beam through magnetic lensing to increase thruster performances [17]. All the above implies that simulation tools need to be able to handle correctly very different magnetic field configurations which, for example, may be non-regular (if they include singular points). Different numerical meshes have been proposed to address the question of how to do this with the least numerical error. Specifically, posing the solution in a particular mesh may either reduce or contribute to the appearance of noteworthy numerical errors.

Within the plasma space propulsion community, there is an outstanding argument on the order of the error induced when solving for the plasma transport equation using unaligned meshes with the magnetic fields, which is mainly due to the anisotropicity that the confining magnetic field creates over the species in the plasma. Recently, some papers regarding this issue have been published; for instance in [3] S.J. Araki states that the accuracy of the solution is increased using MFA meshes, although errors due to poor quality of the boundary elements might be present despite performing a local refinement. Whereas [18] presents an iterative method to accurately compute electron fluxes in non-aligned meshes with good results.

Precisely, this project is devoted to estimating this diffusion error when projecting the plasma anisotropic diffusion equation onto the local system of coordinates of a non-aligned mesh, through implementation of a Finite Volume Method (FVM) in high-level programming platform, MATLAB®. Thus, giving an insight in the possible benefits of the generation Magnetic Field Aligned meshes despite their

higher cost compared against non-aligned meshes.

The structure of this Bachelor Thesis is organized as follows:

Chapter 2 describes the physical problem: confinement of the plasma due to the magnetic field, and includes the derivation of the plasma anisotropic diffusion equation (see Section 2.1). Additionally, Section 2.2 gathers the numerical modeling of the equations using the FVM technique, in which a separated subsection explores the gradient reconstruction methods employed in the structured and MFA meshes. Finally, a discussion on numerical diffusion is provided.

Chapter 3 presents the obtained results. First, numerical diffusion in a structured, regular, non-aligned mesh will be quantified, followed by a discussion on how may geometric mesh quality affect the solution. Second, benchmark results for the evolution of a highly anisotropic problem in both, non-aligned and aligned meshes will be discussed.

Chapter 4 summarizes the main conclusions of this Bachelor Thesis, in which a preliminary estimation on the budget needed to accomplish this work is included.

Moreover, additional information is included in the following appendices:

Appendix A presents the validation of the code.

Appendix B includes a conference paper on numerical diffusion for highly anisotropic diffusion problems in propulsion plasmas, which contains part of the results of this Bachelor Thesis.

Chapter 2

Numerical modeling and analysis in highly anisotropic systems

The growth in computer power and availability during the past half-century has lead to an increasing use of numerical tools. This has favored the appearance of widely recognized platforms available for the implementation of algorithms. Among the more extensively used programming languages, MATLAB® (MATrix LABoratory) offers a numerical computing environment mostly intended for algorithm implementation with efficient matrix handling, as well as providing resources for big data storage in scientific and engineering formats, as for example, HDF5 (Hierarchical Data Format).

As part of the development of the new generation of electric propulsion engines, numerical models and simulations are being developed to be extensively use on the design of said devices. The present project deals with the numerical analysis of highly anisotropic magnetized plasmas, and this chapter is intended to give the reader an understanding on the modeling of the equations used to obtain the results presented in Chapter 3.

2.1 The physical problem: confinement of the plasma due to the magnetic field

In general terms, plasma is considered to be an ionized gas. According to [19] this fourth state of matter is reached when the temperature of a gas is increased sufficiently so that high energy collisions among the atoms cause the electrons to detach; thus, leading to ions. For the particular case of an EP device, generation of plasma is not only done via thermal heating of the propellant, but also due to enforced electron collisions with the atoms of the gas, as was discussed in Section

1.2.1.

In this way, different species may appear in a neutral plasma that should be considered for the formulation of the problem: neutral atoms, ions and electrons; the main separation in EP thrusters comes in terms of "magnetized" (confined) populations and those which are unmagnetized. Furthermore, instead of considering plasma as a collection of individual particles, it is possible to model the behaviour of certain populations as a fluid using the magnetohydrodynamics (MHD) equations [19]. Notice that the interest lies on the macroscopic changes rather than on the individual effects that occur at the particle level.

The presence of the magnetic field in an electromagnetic thruster has as a result the confinement of some of the species in the plasma (usually electrons, ions are only confined in the VASIMR). Following a typical assumption in the analysis of EP plasmas, the confined population can be treated as a highly anisotropic fluid satisfying the maxwellian distribution functions. This anisotropicity is modeled by the transport coefficients perpendicular and parallel to the magnetic field; with the perpendicular transport coefficient scaled with B^{-2}, and generally at least one order of magnitude smaller than the parallel electron transport coefficient [3].

For example, in the case of the electrons, the gyroradius is very small compared to the thruster (because of their small mass) and thus are subjected to the gyromotion, which confers them to the thruster. Collisions account for transport in the perpendicular direction while the parallel motion is "unbounded" by the magnetic field. On the contrary, ions are considered unmagnetized by the magnetic field because of their much larger gyroradius ($\sim 1m$ for typical magnetic field).

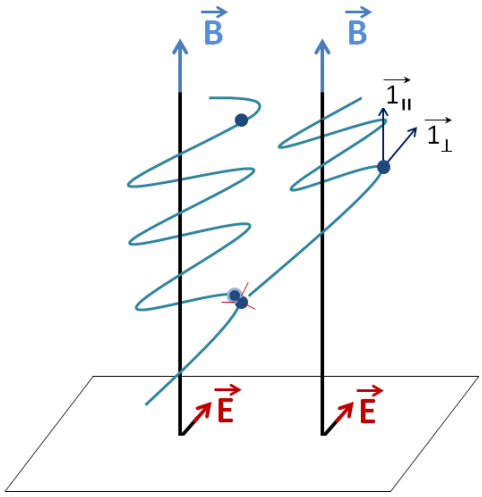

Figure 2.1: Confinement of the electrons due to the $\vec{E} \times \vec{B}$ drift

Specifically, the physical meaning of the transport coefficients is due to the interaction of the plasma with the magnetic field. If we consider an electron moving in the presence of a uniform magnetic field, it will be able to freely move parallel to

the magnetic field lines ($\vec{1}_{\parallel}$), but its motion will be restricted in the perpendicular direction ($\vec{1}_{\perp}$); the $\vec{v} \times \vec{B}$ product results in a force in the direction perpendicular to $\vec{B}$ (see Equation 1.1). If we now consider the presence of an electric field, as depicted in Figure 2.1, the $\vec{E} \times \vec{B}$ drift will act on the velocity component of the particle perpendicular to the magnetic field, but the motion of the confined electron will be unbounded in the direction parallel to it ($\vec{1}_{\parallel}$). Therefore, the gyromotion will confer them to the filed lines, and diffusion to nearby magnetic field lines may only occur through collsions.

It should be stated that the formulation of the anisotropic diffusion equation, which will be derived in Section 2.1.1 according to the model by Simon [20], does imply a plasma with all the species (ions and electrons) confined.

2.1.1 Anisotropic plasma diffusion equation

If we consider a domain in which plasma is non-uniformly distributed, there will be a random motion of particles resulting in a migration from the highest-density to the lowest-density region trying to compensate for the density gradient. This migration is known as diffusion. In a plasma subjected to a magnetic field the mechanism suffers from anisotropicity.

The time dependent equations for the electron and ion densities, respectively, can be obtained starting from continuity equation and following a formal derivation by Simon [20].

Considering an infinite slab problem in which there is a magnetic field in the y'-direction and an electric field perpendicular to it, in the x'-direction, the equations for each species read:

$$\frac{\partial n_e}{\partial t} = D_{\perp e}\frac{\partial^2 n_e}{\partial x'^2} - \mu_{\perp e}\frac{\partial}{\partial x'}(n_e E_{x'}) + D_{\parallel e}\frac{\partial^2 n_e}{\partial y'^2} - \mu_{\parallel e}\frac{\partial}{\partial y'}(n_e E_{y'}) \tag{2.1}$$

$$\frac{\partial n_i}{\partial t} = D_{\perp i}\frac{\partial^2 n_i}{\partial x'^2} - \mu_{\perp i}\frac{\partial}{\partial x'}(n_i E_{x'}) + D_{\parallel i}\frac{\partial^2 n_i}{\partial y'^2} - \mu_{\parallel i}\frac{\partial}{\partial y'}(n_i E_{y'}) \tag{2.2}$$

Where the suffixes e and i refer to the electrons and ions, respectively. For each of them: n is the density, μ is the mobility coefficient, and $D_{\perp}$ and $D_{\parallel}$ denote, respectively, the diffusion of each species across the magnetic field (due to collision mechanisms) and along the magnetic field lines (natural diffusion). $E_{x'}$ and $E_{y'}$ are the components of the electric field in the plasma.

An accepted approach to eliminate the dependency of the $E_{x'}$ component of the

electric field is to assume that the ratio of both electric field components is similar to the ratio of the dimension of the domain in the x' direction, R, to the dimension in y', L:

$$\frac{E_{y'}}{E_{x'}} \sim \frac{R}{L} \tag{2.3}$$

Which is due to the fact that the electric field is the derivative of the scalar electric potential ($\vec{E} = -\vec{\nabla}\phi$), which varies from a positive value at the center to a zero at the walls. Therefore, unless provided a sufficiently thin an long domain, the electric field component in the direction perpendicular to the magnetic field, Ex', can be assumed to vanish. In other words, space charge neutrality will be provided by currents flowing along y'.

To avoid explicitly having a dependency on $E_{y'}$ it is possible to rearrange Equations 2.1 and 2.2. Firstly, assuming a quasineutral plasma ($n_e \approx n_i$) both equations will be of the form:

$$\frac{\partial n}{\partial t} = D_e \nabla^2 n - \mu_{\parallel e} \frac{\partial}{\partial y'}(n E_{y'}) \tag{2.4}$$

$$\frac{\partial n}{\partial t} = D_i \nabla^2 n - \mu_{\parallel i} \frac{\partial}{\partial y'}(n E_{y'}) \tag{2.5}$$

Multiplying Equation 2.2 by $\mu_{\parallel i}$ and Equation 2.5 by $\mu_{\parallel e}$, and substracting them, the following expression is obtained:

$$\frac{\partial n}{\partial t} = \begin{bmatrix} \frac{\mu_{\parallel e} D_{\perp i} - \mu_{\parallel i} D_{\perp e}}{\mu_{\parallel e} - \mu_{\parallel i}} & 0 \\ 0 & \frac{\mu_{\parallel e} D_{\parallel i} - \mu_{\parallel i} D_{\parallel e}}{\mu_{\parallel e} - \mu_{\parallel i}} \end{bmatrix} \begin{bmatrix} \frac{\partial^2 n}{\partial x'^2} \\ \frac{\partial^2 n}{\partial y'^2} \end{bmatrix} \tag{2.6}$$

It is important to notice that the diffusion parallel to the magnetic field (along y'-axis) is equal to the ambipolar coefficient, which is given by:

$$D_A = \frac{\mu_{\parallel e} D_{\parallel i} - \mu_{\parallel i} D_{\parallel e}}{\mu_{\parallel e} - \mu_{\parallel i}} \tag{2.7}$$

The following dictates that, parallel to the magnetic field, electrons and ions diffuse with the same ambipolar diffusion coefficient, D_A, which gathers two main effects: their own "free" diffusion, and the suffered deceleration or acceleration due to the

self generated ambipolar electric field (which makes the flux, and therefore the diffusion rate, of both species become equal).

Analogously, the diffusion coefficient perpendicular to the magnetic field, in the x'-direction, will be given by:

$$D_{x'} = \frac{\mu_{\|e} D_{\perp i} - \mu_{\|i} D_{\perp e}}{\mu_{\|e} - \mu_{\|i}} \tag{2.8}$$

Note that this coefficient is essentially $D_{x'} = D_{\perp i}$ since the confinement of electrons due to the presence of the magnetic field forces $D_{\perp e} \ll D_{\perp i}$ and, in general, $\mu_{\|e} \gg \mu_{\|i}$.

As we are only interested in the numerical error induced by anisotropicity, this effect in the plasma will be modeled to be given by $D_{\|}$ and $D_{\perp}$. These simplified diffusion terms account for the parallel and perpendicular directions to the magnetic field, respectively. Following this reasoning, the problem reduces to:

$$\frac{\partial n}{\partial t} = \nabla' \cdot (D' \nabla' n) = \nabla' \cdot \vec{\Gamma'} = \nabla' \cdot \begin{bmatrix} \Gamma_{x'} \\ \Gamma_{y'} \end{bmatrix} \tag{2.9}$$

Where the term $\vec{\Gamma'}$ accounts for the flux of each species, the nabla operator ∇' is expressed in the coordinates defined by the local directions of the magnetic field, and D' is the anisotropic diffusion term expressed as:

$$D' = \begin{bmatrix} \frac{\mu_{\|e} D_{\perp i} - \mu_{\|i} D_{\perp e}}{\mu_{\|e} - \mu_{\|i}} & 0 \\ 0 & \frac{\mu_{\|e} D_{\|i} - \mu_{\|i} D_{\|e}}{\mu_{\|e} - \mu_{\|i}} \end{bmatrix} = \begin{bmatrix} D_{\perp} & 0 \\ 0 & D_{\|} \end{bmatrix} \tag{2.10}$$

The form in which the diffusion term is specified will allow to tweak the plasma transport by modifying the perpendicular and parallel diffusion coefficients. The anistropicity of the problem can be modeled as the ratio of both diffusion coefficients, given by Θ:

$$\Theta = \frac{D_{\|}}{D_{\perp}} \tag{2.11}$$

It is readily inferred that the larger the diffusion ratio is, the higher the anisotropic nature of the problem (provided that $D_{\|} \gg D_{\perp}$). On the extreme of $D_{\|}$ finite and $D_{\perp} = 0$ the diffusion ratio will be maximum ($\Theta \to \infty$). Physically, this will mean that the gyromotion of the plasma in which only an ambipolar electric field arises, is constrained to be parallel to the magnetic field lines, and a density gradient across such lines should not appear.

Equation 2.9may be used when solving for the anisotropic plasma transport in the MFA mesh since the equation is already expressed in the curvilinear coordinates aligned with the directions perpendicular and parallel to the magnetic field, given by the versors $(\vec{1_\perp}, \vec{1_\parallel})$.

However, the numerical diffusion problem arises when Equation 2.9 is projected onto a coordinate system not aligned with that of the magnetic field. To that end, and following a similar reasoning as in [21], the diffusion equation will be discretized in a new coordinate system such as a cartesian, whose principal directions will be given by x and y. Specifically, the magnetic field lines will be considered to be straight lines, being the magnetic versors $\vec{1_\perp}$ and $\vec{1_\parallel}$ rotated an angle α with respect to the new system. This approach will enable us to later extrapolate and generalize the problem to a curved magnetic field, where at each point of the domain given by (x_0, y_0) the "local" angle of the magnetic field lines, α, can be calculated.

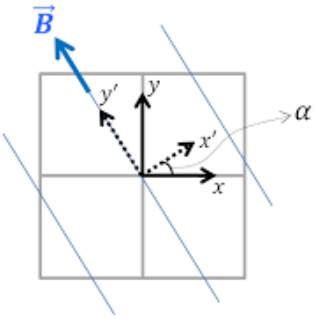

Figure 2.2: Magnetic field orientation with respect to cartesian coordinate system

As depicted in Figure 2.2, defining α as the angle between the magnetic field (x', y') and the cartesian coordinate system (x, y) it is possible to use a rotation matrix, R, to define the diffusion tensor, and consequently the flux, in the cartesian system using the following relations:

$$R = \begin{bmatrix} \cos\alpha & -\sin\alpha \\ \sin\alpha & \cos\alpha \end{bmatrix} \tag{2.12}$$

$$\vec{\Gamma} = R \cdot \vec{\Gamma'} \tag{2.13}$$

$$\nabla' n = R \cdot \nabla n \tag{2.14}$$

Applying previous relations, the discretized diffusion equation reads:

$$\frac{\partial n}{\partial t} = \nabla \cdot [R^{-1} D' R \cdot \nabla n] \tag{2.15}$$

Where the nabla operator, ∇, is now in the (x, y) cartesian system. Therefore, the resulting diffusion term will be given by:

$$D = R^{-1}D'R = \begin{bmatrix} D_\perp \cos^2\alpha + D_\parallel \sin^2\alpha & (D_\parallel - D_\perp)\cos\alpha\sin\alpha \\ (D_\parallel - D_\perp)\cos\alpha\sin\alpha & D_\parallel \cos^2\alpha + D_\perp \sin^2\alpha \end{bmatrix} \tag{2.16}$$

In a first approach, the arising diffusion term differs from Equation 2.10 (used when solving the diffusion equation in the curvilinear magnetic coordinates); as the diagonal and off-diagonal terms are neither null nor given by the diffusion coefficients, $D_\perp$ or $D_\parallel$, but depend on the orientation of the field lines, α. It is due to these terms that numerical diffusion will arise; a more detailed discussion will be done when dealing with the numerical discretization of the equation (Section 2.2.2).

2.2 Numerical methods

This section presents the numerical discretization of the anisotropic diffusion equation 2.15. To that end, the mostly accepted discretization methods will be presented, followed by a discussion on the chosen techniques through which the equation will be discretized. Finally, a detailed explanation on the numerical modeling of the equation is provided.

2.2.1 Discretization techniques

FVM and FEM formulations

There are several techniques developed to discretize and numerically solve Partial Differential Equations (PDEs). Among them, both, Finite Element Method (FEM) and Finite Volume Method (FVM) have shown to provide accurate solutions for a broad scope of problems. In addition, the use of these two highly versatile numerical tools is widely extended in Computational Fluid Dynamics (CFD) software, where depending the type of problem, one method or even a hybrid model of both is normally used to obtain a numerical answer. The principle in which both are based lies on the spatial discretization of the domain to be analyzed by subdividing it on smaller mesh elements.

The concept of a FEM is to solve a weak form of the PDE (simple equations that approximate the equation to be solved) by minimizing the approximation residual error instead of directly solving the original and more complex equation. The final result leads to a set of algebraic equations for the obtained approximate solutions

which are calculated from the initial values of the problem. The most well-known practical application of a FEM solver is the Finite Element Analysis (FEA).

On the contrary, the FVM approach uses the integral form of the conservation equations as the starting point. The domain is subdivided in elements to which conservation equations are applied. These volumes are identified by their respective center points, and the required information of the neighbour cells is considered at the element facets. This method is conservative by definition because of the form in which the equation is discretized, by which the divergence term is evaluated as fluxes at the facets of each element. This guarantees a conservative or "strong" approach throughout the domain since, for a given volume, the fluxes entering are necessarily equal to the fluxes leaving the adjacent mesh element.

In overall, the implementation of a Finite Element Method will require more complex codes according to the followed steps, increasing the needed computational time. Otherwise in FVM, interpolation is only required between cells and nodes, notwithstanding, the computational time will be given by the order of accuracy of the scheme used to discretize the PDE. Despite both techniques being able to cope with complex geometries using unstructured grids, FVM are preferred when dealing with conservation equations since, as mentioned, FEM solves a weak form of the Partial Differential Equation [22] [23].

Therefore, since a conservative method is required for the modeling of the anisotropic diffusion equation (Equation 2.9) it can be clearly understood why the numerical discretization of such will be done by means of a FVM technique.

Explicit and Explicit schemes

Attending to the time-stepping schemes either an implicit or an explicit time discretization method needs to be followed.

Explicit algorithms are usually readily coded and, in general, will require lest amount of computational resources. The main set-back is the required time step that ensures stability, which is mainly dependent on the mesh size. Specially, it will necessarily be smaller when there exists a high degree of disparity among the sizes of the individual volumes.

Conversely, the cost per time step of an implicit scheme is much higher, fostered by the underlying complexity of the discretization procedure of the PDE. Most of the implicit schemes are conditionally stable over a wide range of time steps, enabling the use of larger time steps in the finding of a solution.

A common procedure is to start the simulation with an explicit method and switch to an implicit scheme once stability is assessed. For the numerical simulation of

the equation of interest (Equation 2.9) an explicit Euler method will be chosen since we are interested in obtaining an accurate temporal evolution rather than the steady-sate solution.

The explicit Euler method is a first order method that approximates the solution to the differential equation at time $t = t_0 + \Delta t$. For the initial value problem: $y' = f(t, y(t))$ with $y(t_0) = y_0$, the method formulates the solution after a time step as:

$$y_{t=t_0+\Delta t} = y_{t_0} + \Delta t f(t_{t_0}, y_{t_0}) \tag{2.17}$$

The stability condition of the discretized anisotropic plasma diffusion equation (Equation 2.21) is provided in Section A.2

2.2.2 Numerical modeling of the anisotropic plasma diffusion equation

The Finite Volume Method requires to reformulate the obtained diffusion equation (Equation 2.9) by integrating over the control volume corresponding to the facets of each mesh element:

$$\int_V \frac{\partial n}{\partial t}\, dV = \int_V \nabla \cdot (D \cdot \nabla n)\, dV \tag{2.18}$$

Where the right-hand side term can be simplified to a closed integral over the area of each element facet by applying the Gauss divergence theorem:

$$\int_V \frac{\partial n}{\partial t}\, dV = \oint_A (D \cdot \nabla n)\, d\vec{A} \tag{2.19}$$

Previous equation is discretized by means of an explicit Euler method. The integrals over volumes and over areas are approximated, respectively, as the value of the function at the center point of the element multiplied by its volume, and as the value of the function at the center of the facet multiplied by the dot product of the area of the facet and its normal vector:

$$\begin{aligned} \int_{V_{e,i}} f\, dV &\approx f_{e,i} \cdot V_{e,i} \\ \int_{A_{f,j}} f\, d\vec{A} &\approx f_{f,j} \cdot A_{f,j} \cdot \vec{n} \end{aligned} \tag{2.20}$$

Therefore, yielding to the following expression that must be satisfied for every mesh element:

$$V_e \frac{n_{e,i}^{t+\Delta t} - n_{e,i}^{t}}{\Delta t} = \sum_j \left((D \cdot \nabla n)|_{f,j} \cdot dA_{f,j} \cdot \vec{n_{f,j}} \right) \tag{2.21}$$

The term $(D \cdot \nabla n)|_{f,j}$ will be expressed as in Equation 2.22 when solving the anisotropic diffusion problem in the MFA mesh meanwhile Equation 2.23 will be necessary for the case of the non-aligned mesh.

$$(D \cdot \nabla' n)|_{f,j} = \left[\begin{array}{c} D_\perp \frac{\partial n}{\partial x'} \\ D_\parallel \frac{\partial n}{\partial y'} \end{array} \right] \Bigg|_{f,j} \tag{2.22}$$

$$\begin{aligned} &(D \cdot \nabla n)|_{f,j} = \\ = &\left[\begin{array}{c} (D_\perp \cos^2\alpha + D_\parallel \sin^2\alpha) \frac{\partial n}{\partial x} + ((D_\parallel - D_\perp)\cos\alpha \sin\alpha) \frac{\partial n}{\partial y} \\ ((D_\parallel - D_\perp)\cos\alpha \sin\alpha) \frac{\partial n}{\partial x} + (D_\parallel \cos^2\alpha + D_\perp \sin^2\alpha) \frac{\partial n}{\partial y} \end{array} \right] \Bigg|_{f,j} \end{aligned} \tag{2.23}$$

Here e, i represents the i^{th} element and f, j the j^{th} facet of the element of interest. The normal vector to the element facet, $\vec{n}$, pointing outward the element volume, as typical in the Gauss theorem.

The conservation property of the FVM formulation can be even more clearly understood by analyzing the equations, in which the flux through any interior face participates in the calculation twice: once for the concerned cell and once for the adjacent cell. Hence the sum of the fluxes either entering or leaving each element volume over the whole computational domain vanishes if zero flux is set as the corresponding boundary condition throughout the domain boundaries.

Numerical Diffusion in non-aligned meshes

If Equations 2.22 and 2.23 are compared against each other it becomes clear that a transfer of mass is enhanced in the later even for the most restrictive case of

$D_\perp = 0$; that is when the plasma is "perfectly" confined.

In fact, for a highly anisotropic plasma and magnetic field orientation, $\alpha \neq 0^o$, two effects may contribute to numerical diffusion: first, the cross-terms induce an undesirable transfer of mass along the element facets (i.e.: between the nodes) when none should occur, as the magnetic field lines should remain impermeable to the plasma if $\Theta \to \infty$. Second, in each iteration, the misalignment between the magnetic field lines and the computational grid causes mass to be transferred across the element facets between contiguous cells, leading to unbounded numerical errors in the solution.

It is also important to notice that if $\alpha = 0^o$ (no grid misalignment) or $D_\parallel = D_\perp$ we will recover the same expression as in Equation 2.22, and no error would appear. Nonetheless, the case in which both diffusion coefficients are equal is far from being highly anisotropic.

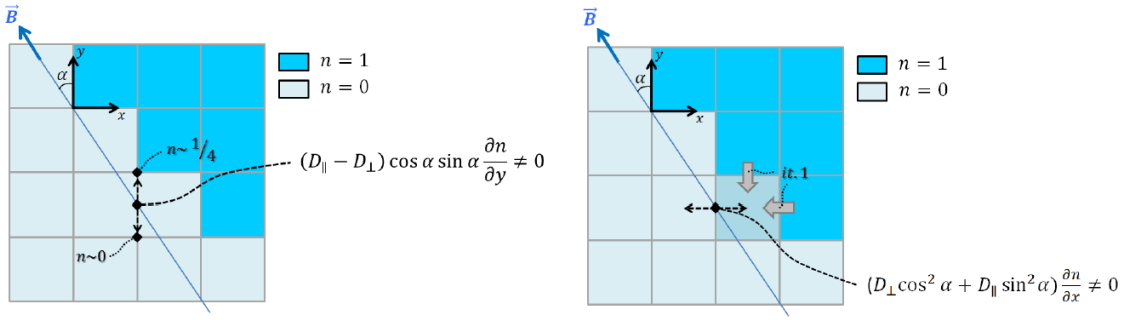

Figure 2.3: Sketch on numerical diffusion

This can be more clearly seen in Figure 2.3, where the gradients along and across the faces both induce a transfer of mass between the nodes and elements that contributes to the undesirable numerical diffusion.

2.2.3 Gradient reconstruction methods

This section is intended to give an insight in the gradient reconstruction methods employed when solving the diffusion equation in the different types of structured meshes and in the non-structured MFA mesh, as well as to comment on the order of error committed.

Gradient reconstruction at the element facets is required in order to approximate the partial derivatives along the principal directions in both the not-aligned and MFA meshes. In an effort to reduce the errors to improve the accuracy of the simulations, the GR algorithm was different attending to the nature of each mesh: in the non-aligned case, a structured mesh can be produced with good

regularity and mesh quality properties. However, aligned meshes need to conform to multiple magnetic topologies and arbitrary domain boundaries, requiring of an "unstructured" approach in which geometric quality and gradient reconstruction accuracy may become a source for error. Indeed discussions on the GR methods focus on the error committed due to low geometric quality mesh regions, and the various methods to generate high order accuracy solutions [24].

Structured mesh

The structured mesh allows us to take advantage of the alignment of the faces of each individual volume element with the cartesian coordinate system formed by x and y. Therefore permitting the modeling of the partial derivatives with respect to said coordinates by a central difference scheme, which leads to a second-order accurate discretization for regular meshes.

Figure 2.4 presents an arbitrarily curved magnetic field in a structured, regular non-aligned mesh, as well as a detail of a mesh element showing the misalignment between the grid coordinates and the magnetic field.

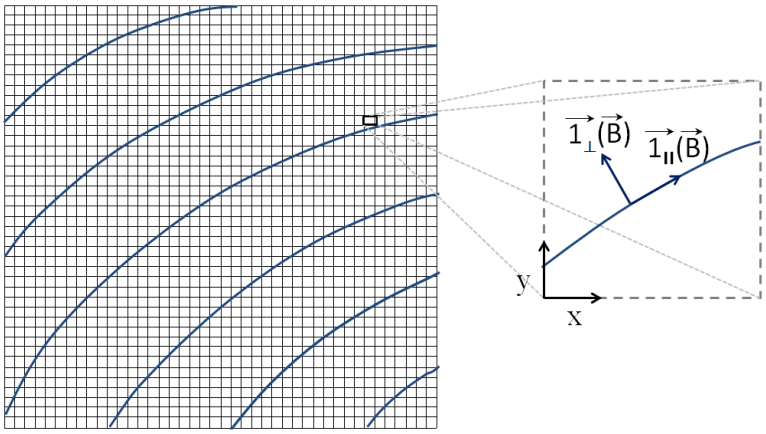

Figure 2.4: Curved magnetic field in a non-aligned mesh

For a face parallel to the y-axis the transfer of mass across the element face will be given by the difference in density between the concerned and contiguous cells over the distance between the center points of each cell:

$$\frac{\partial n}{\partial x} \approx \frac{n_2 - n_1}{\Delta x} \tag{2.24}$$

Notice that the definition of n_2 and n_1 is not trivial and must be established in accordance with the sign criteria given by the (x, y) coordinate system, which defines the direction of the gradient. A positive flux implies a gain of mass

while a negative supposes a transfer of mass to contiguous cells. For the analysis concerned, the notation of the adjacent elements is established as depicted in Figure 2.5.

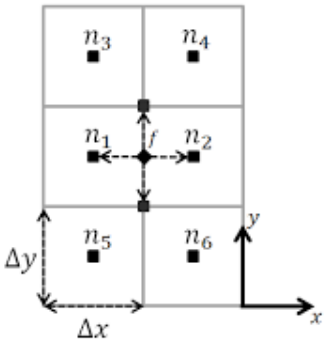

Figure 2.5: Central Differences

The gradient along the faces is approximated in a similar form, by a central difference scheme at the face nodes [21]:

$$\frac{\partial n}{\partial y} \approx \frac{n_{node_2} - n_{node_1}}{\Delta y} \tag{2.25}$$

The density at the nodes can be interpolated from surrounding elements by means of a weighted mean. In order for the algorithm to be versatile and allow accurate gradient reconstruction in regions with dissimilar mesh refinement, each element or stencil point considered for the interpolation will appear multiplied by a coefficient, to assign different weights to each stencil depending on the distance from the element center to the node:

$$n_{node} \approx \sum_{i=1}^{s} c_i n_i \tag{2.26}$$

Being s the number of stencil points considered; with the coefficients satisfying:

$$c_i = \frac{1/d_i}{\sum_{i=1}^{s}(1/d_i)} \tag{2.27}$$

Thereby, in the case of a structured, regular mesh, all the coefficients will be equal to 1/4 in the case of a node surrounded by four mesh elements.

MFA mesh

In order to apply Equation 2.9 in an arbitrarily curved magnetic field, we will use the magnetic curvilinear coordinates defined by the scalar potential and stream functions. These functions are derived from their relations with the magnetic field, which is considered to be irrotational ($\nabla \times \vec{B} \approx 0$), solenoidal ($\nabla \cdot \vec{B} = 0$), and stationary ($\frac{\partial \vec{B}}{\partial t} = 0$).

The irrotational approximation can only be applied in case the currents generated in the thrusters have little effect in altering the magnetic field imposed by an external magnetic circuit. This is the case in most electromagnetic thrusters detailed in Section 1.2.1, with the exception of some MPDs and the VASIMR.

Under these assumptions, a curvilinear system of coordinates in the local magnetic field directions can be obtained for an axisymmetric domain, defined by the cylindrical coordinates R and Z:

$$\nabla \cdot \vec{B} = 0 \rightarrow \nabla^2 \lambda = 0 \rightarrow \frac{\partial \lambda}{\partial r} = -rB_z; \frac{\partial \lambda}{\partial z} = rB_z \tag{2.28}$$

$$\nabla \times \vec{B} \approx 0 \rightarrow \nabla \sigma = \vec{B} \rightarrow \frac{\partial \sigma}{\partial r} = B_r; \frac{\partial \sigma}{\partial z} = B_z \tag{2.29}$$

A MFAM for an arbitrarily curved magnetic field is depicted in Figure 2.6. The MFA mesh is defined by lines of constant λ, which are parallel to the local magnetic versor $\vec{1}_{\parallel}$, and lines of constant magnetic potential, σ, locally aligned with the perpendicular direction of the magnetic field, $\vec{1}_{\perp}$.

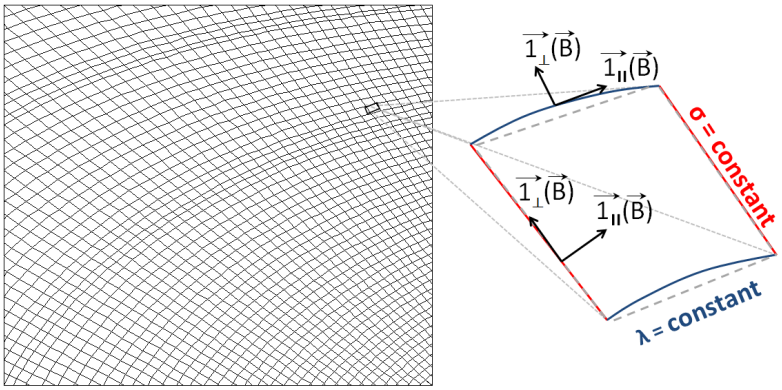

Figure 2.6: MFAM for a curved magnetic field

In this coordinate system we may apply the discretization given by Equation 2.9, where the gradients are with respect to the magnetic curvilinear coordinates:

$$\nabla' n = B\frac{\partial n}{\partial \sigma}\,\vec{1}_{\parallel} + rB\frac{\partial n}{\partial \lambda}\,\vec{1}_{\perp} \tag{2.30}$$

If it is intended to reproduce the GR method of central differences in the MFAM, Equation 2.24 needs to be projected onto the normal direction of the element facet to take into account misalignment. However, this method was followed in [3] and preferable results were obtained if such misalignment was disregarded. Consequently, this highlights the need of a higher order differencing schemes when dealing with non-structured meshes. In an effort to reduce the errors arising from the numerical discretization of the partial derivatives, an equivalent method to the Weighted Least Squared (WLSQR) described in [24] was already implemented in the code used for GR in the MFA mesh: the WLSQR Face Interpolation.

The method is based on a Taylor series expansion that approximates the value of a certain function, ϕ, as well as its derivatives and cross-derivatives, at the facet center from the value of said function at a set of stencil points; these stencils are at the center of the surrounding elements. Typically, several weighting factors can be defined to distinguish among the different stencils, which can be functions of inverse distance, element area or any other desired combination. Following this reasoning, the gradients along the local directions given by $\vec{1}_{\parallel}$ and $\vec{1}_{\perp}$, respectively, are be approximated as:

$$\begin{aligned} \nabla_{\sigma} n &= B\frac{\partial n}{\partial \sigma}\,\vec{1}_{\parallel} \approx B\sum_{i}^{s} c_i n_i\,\vec{1}_{\parallel} \\ \nabla_{\lambda} n &= rB\frac{\partial n}{\partial \lambda}\,\vec{1}_{\perp} \approx rB\sum_{i}^{s} c_i n_i\,\vec{1}_{\perp} \end{aligned} \tag{2.31}$$

Being s the number of stencil points considered, and c_i the value of the coefficient for the i^{th} stencil point.

The versatility of the WLSQR allows to readily adjust the GR quality in the MFA mesh by selecting the order of the Taylor expansion, as well as to tweak the results by assigning different weighting options. The algorithm compares the output of the GR method against a set of functions (linear, quadratic, cubic, sinusoidal, etc.), and returns the relative error for each of them. For the studied problem geometry, it was found that a Taylor expansion of order 1 and inverse distance weighting yielded better results (see Section 3.2.2).

Chapter 3

Results

The obtained results have been gathered in this chapter, which is divided into two main parts. Firstly, numerical diffusion in the structured, regular mesh will be quantified, followed by a discussion on the effect that geometric mesh quality might have on the solution. The second part is devoted to the comparison of a highly anisotropic problem in the structured mesh against the non-structured MFAM, to be able to conclude whether or not the error arising from gradient reconstruction and mesh irregularities in the MFAM will be of the same order of magnitude than the error induced by numerical diffusion.

3.1 Anisotropic diffusion problem in structured meshes

3.1.1 Regular meshes

To prove the presence of numerical diffusion, the anisotropic plasma diffusion equation has been solved in a structured, regular mesh. For a mesh resolution of 500 elements, Figure 3.1 shows the evolution of a perfectly anisotropic system ($\Theta \to \infty$) in an arbitrarily large domain with non-permeable walls, in which the magnetic field lines are unaligned with the computational grid ($\alpha = -45^{o}$). Note that the density (n') is adimensionalized with a reference density $n = 1 \cdot 10^{17}\, m^{-3}$, and t' is the number of iterations.

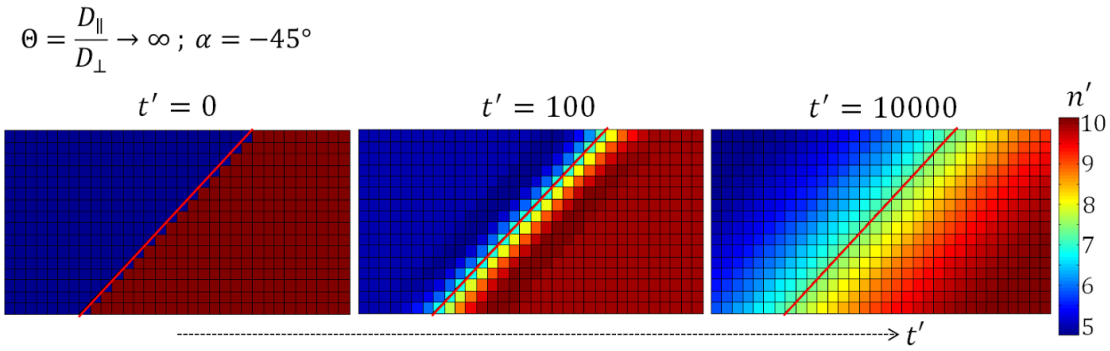

Figure 3.1: Evolution of numerical diffusion

A low density region and a high density region are set as the initial conditions, at t'=0. As it was expected, numerical diffusion appears as the simulation progresses. The "last" magnetic field line separating both initial regions, depicted in red, should not allow any transfer of mass across it; the condition in this particular case of $D_\perp = 0$ ($\Theta \to \infty$) should imply having both plasma regions perfectly confined.

It is possible to quantitatively assess how the magnetic field orientation and mesh refinement contribute to numerical diffusion by means of an average error, which is quantified only considering the affected mesh elements (in this case, those on the left of the depicted magnetic field line):

$$< error(t) >= \frac{1}{N_{elem}} \sum_{i=1}^{N} \frac{|n_i(t) - n(t=0)|}{n(t=0)} \tag{3.1}$$

The evolution of this average error is shown in Figure 3.2. An important conclusion to be extracted from Figure 3.2b is that, although for sufficiently large times the solution will diverge, a higher mesh resolution leads to a partial containment of the error. This will latter be used to give an idea on the order of elements needed for a solution in a structured mesh to be comparable to that of the non-structured MFA mesh, which is, by definition, free from numerical diffusion (although it may present typical numerical discretization errors).

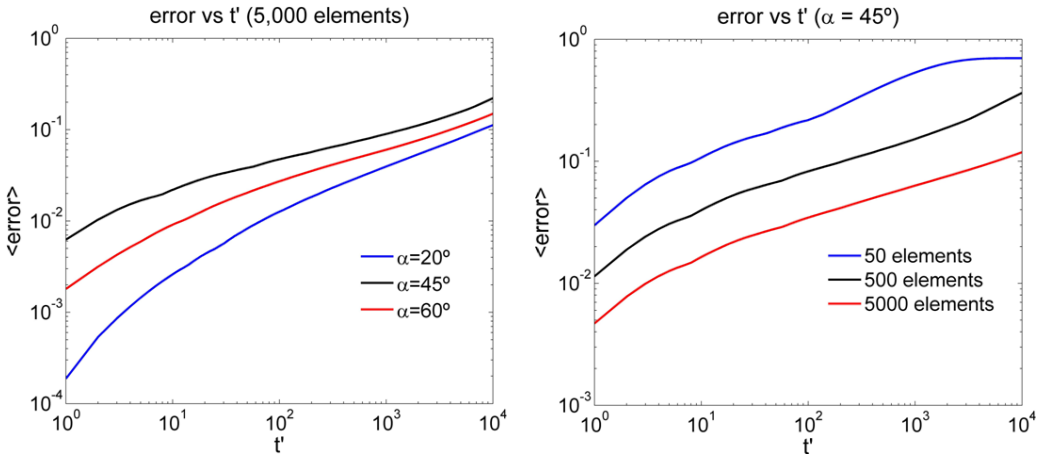

(a) Error vs. t' for different magnetic field orientation, α

(b) Error vs. t' for different mesh resolution

Figure 3.2: Error vs t' ($\Theta \to \infty$)

A more qualitative approach may aid to have a better understanding of numerical diffusion. With this purpose, it is useful to introduced an "effective diffusion coefficient ratio", Θ_{eff}. For a given domain, number of elements and initially equal low and high plasma density regions, we can consider two different problems: the first case with a diffusion coefficient (Θ) in which the computational grid is at a certain angle with the magnetic field (α), and an analogous problem with $\Theta = \Theta_{eff}$ and $\alpha = 0^o$. In this case, Θ_{eff} is defined as the ratio of diffusion coefficients that produces an equivalent diffusive mass flux between the different plasma density regions to the non-aligned problem. Table 3.1 presents the effective diffusion coefficient in various conditions due to numerical diffusion.

	$\Theta_{eff} \sim ...$	$\Theta \to \infty$	$\Theta = 100$	$\Theta = 10$
Mesh Resolution = 50 elements	$\alpha = 20^o$	~ 5	~ 4	~ 3
	$\alpha = 45^o$	~ 5	~ 5	~ 3
	$\alpha = 60^o$	~ 5	~ 5	~ 3
Mesh Resolution = 500 elements	$\alpha = 20^o$	~ 20	~ 15	~ 5
	$\alpha = 45^o$	~ 25	~ 15	~ 5
	$\alpha = 60^o$	~ 20	~ 15	~ 6
Mesh Resolution = 5,000 elements	$\alpha = 20^o$	~ 50	~ 25	~ 8
	$\alpha = 45^o$	~ 50	~ 30	~ 8
	$\alpha = 60^o$	~ 50	~ 30	~ 7

Table 3.1: Effective Diffusion Coefficient ratio, Θ_{eff}, for different mesh resolutions, alignment of the magnetic field (α) and diffusion coefficient ratios (Θ)

Results showed to be in agreement with [25] and [26]. In regards of Table 3.1, errors committed due to misalignment are nearly independent on the orientation of the magnetic field. It is also evidenced that numerical diffusion contributes to a reduction in the anisotropicity of the system, being this effect more noticeable if the degree of anisotropicity is high, showing a non linear relation between the Θ_{eff} and the actual anisotropicity simulated in the problem; in these cases an increased mesh resolution aids, up to some extent, to reduce numerical diffusion.

3.1.2 Non-Regular meshes

Previous discussions on mesh quality of the structured mesh have only been focused on mesh resolution. However, we are also interested in exploring the effect of geometric mesh quality on numerical diffusion. This is because we are aware of discretization errors due to bad mesh quality in the MFAM being a source of error, and we wish to understand what the effects of a non-regular structured mesh might imply for numerical diffusion. With this purpose, three different meshes will be compared: meshes with Regularly, Randomly and Gaussianly distributed mesh nodes.

Geometric mesh quality

For these three meshes, geometric mesh quality has been assessed based on two parameters: smoothness and aspect ratio. Typically, the skewness parameter is also of importance for mesh quality although not in the cases we explore, due to the "rectangular" nature of the mesh elements.

$$smoothness = \frac{max(A_{element}, A_{adjacent})}{min(A_{element}, A_{adjacent})} \tag{3.2}$$

$$aspect\,ratio = \frac{max(facet - length_{element})}{min(facet - length_{element})} \tag{3.3}$$

Here, $A_{element}$ and $A_{adjacent}$ refer to, respectively, the element being considered and the adjacent elements to it. Large values of both parameters will outline the existence of poor quality regions in the mesh. With a mesh resolution of 1,000 elements, Figures 3.3 and 3.4 evaluates both parameters in the Random and Gaussian meshes:

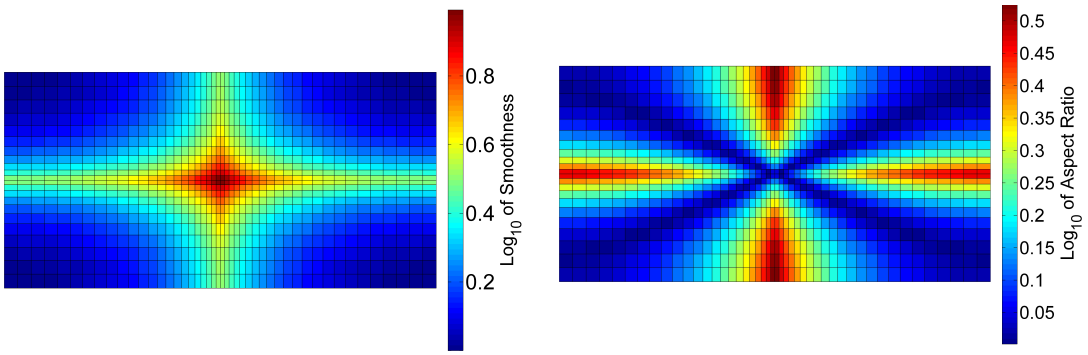

(a) Log_{10} of smoothness (b) Log_{10} of aspect ratio

Figure 3.3: Gaussian mesh

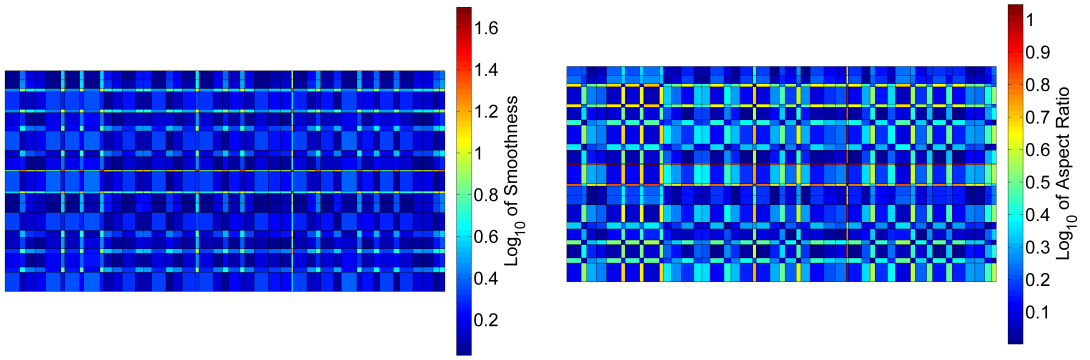

(a) Log_{10} of smoothness (b) Log_{10} of aspect ratio

Figure 3.4: Random mesh

To complement previous figures, Table 3.2 gathers some statistical data:

Parameter	Mesh	Maximum	Minimum	Mean
Log_{10} of Smoothness	Random	1.69	0.11	0.72
	Gaussian	0.99	0	0.38
Log_{10} of Aspect ratio	Random	1.05	0	0.35
	Gaussian	0.53	0	0.19

Table 3.2: Geometric mesh quality: main parameters

Comparison of regular versus non-regular meshes

The comparison among the three meshes has been done in terms of the average error (Equation 3.1). As inferred from Figure 3.5, geometric mesh quality is very unlikely to alter numerical diffusion; the Gaussian mesh results in a slightly large average error in spite of having better values of both parameters than the randomly generated mesh.

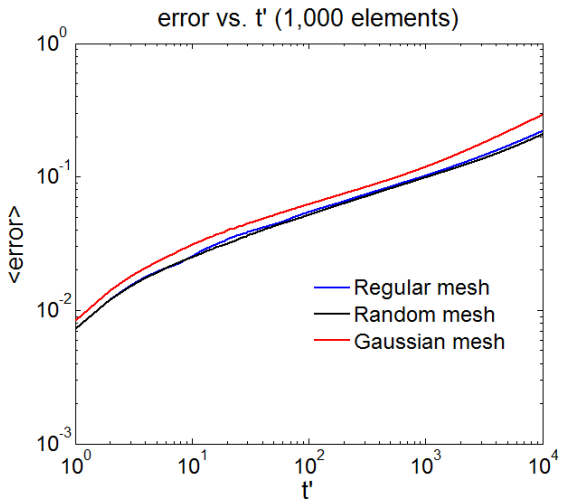

Figure 3.5: Error vs. t', different mesh quality

3.2 Anisotropic diffusion problem in MFA meshes

A MFAM is characterized by having each facet of the computational elements closely aligned with either a λ or σ line, which are, respectively, isolines tangent to the local magnetic field versors $\vec{1}_{\parallel}$ and $\vec{1}_{\perp}$, as depicted in Figure 3.6.

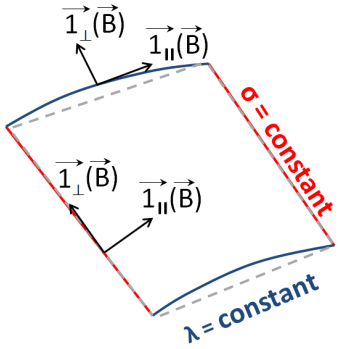

Figure 3.6: Detail of mesh element

MFA meshes are seen to provide a more accurate approach on the modeling of highly anisotropic systems since numerical diffusion, by definition, cannot be present in the solution. However, numerical errors due to low quality regions and gradient reconstruction techniques are potentially comparable to those produced by numerical diffusion. We will argue that by careful generation of the MFAM mesh and correct selection of gradient reconstruction methods these errors will not be comparable to those from numerical diffusion.

3.2.1 MFA mesh generation

Contrarily to a regular mesh, the building of a MFA mesh requires the use of custom techniques able of accurately reproducing a wide variety of magnetic field geometries and, if possible, allowing a post processing for the improvement of certain mesh regions.

The meshing strategies implemented in the Mesh Generator from the NOMADS platform are:

1. Compute the magnetic field in an initial structured mesh

   An initial regular mesh is generated, in which the value of the magnetic field at each point is computed.

2. Integrates λ and σ in the domain

   Making use of the relations of the scalar and stream functions, the values of λ and σ can be computed over the initial mesh.

3. Contour levels generation

   Special care should be paid to extrapolate the values of the magnetic coordinates to build the MFA mesh. This requires the use of suitable spacing methods to avoid the generation of elements with dissimilar size. For example, if contour levels are not correctly chosen, larger elements will appear in regions with low magnetic field strength (i.e.: singular points, local minima) compared to regions with higher magnetic field strength.

   There are several options available that address this issue such as smoothing, which evenly distributes the isolines by means of a least squares method (independent on the local variation of the magnetic field). The logarithmic spacing is used to avoid dissimilar elements in regions with lower magnetic field intensity, tending toward the selection of contour levels for smaller values. The Exponential-stretching proposed by [3] or the "Expanded"-exponential-stretching result in more robust methods, as they achieve initial good quality meshes.

4. Contour level manual correction

   If necessary, the algorithm allows for a manual correction of isolines to improve the spacing of contour levels, specially regarding boundary elements (some of which may have up to 5 facets) through a Graphical User Interface.

5. Generation of MFA mesh

   The MFA data is stored in HDF5 format, structured by elements, facets, nodes, etc.

3.2.2 WLSQR Method for gradient reconstruction in MFA mesh

For the studied problem in Section 3.2.3, gradient reconstruction with a Taylor expansion of order 1 yielded better results than expansions of higher orders. The justification may be provided based in Figures 3.7 and 3.8, where the relative error of the GR method for functions ϕ_1 and ϕ_2 is presented.

$$\phi_1 \sim \lambda + \sigma$$
$$\phi_2 \sim \sin\lambda \cdot \cos\sigma$$

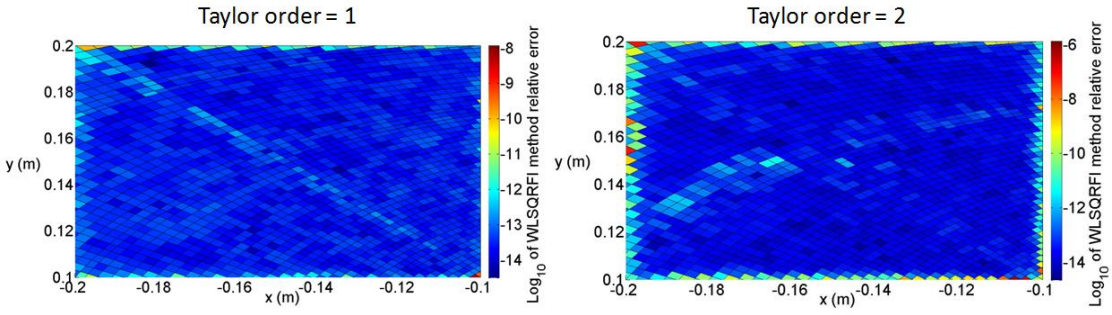

Figure 3.7: Log_{10} of relative error for ϕ_1

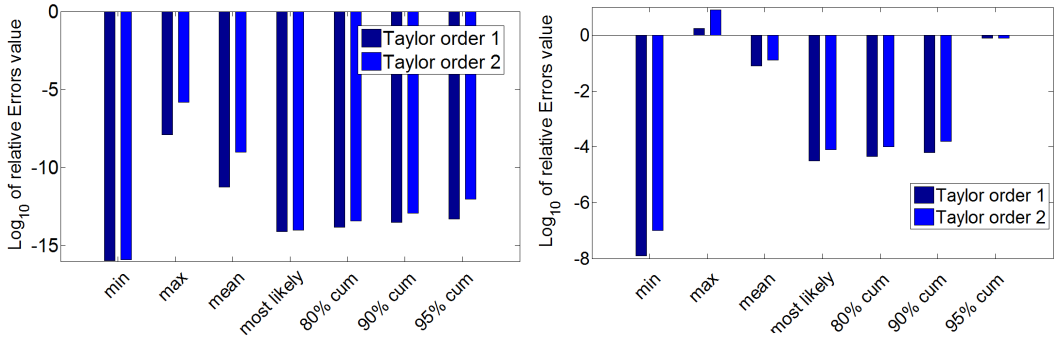

(a) Log_{10} of relative error for ϕ_1 (b) Log_{10} of relative error for ϕ_2

Figure 3.8: Log_{10} of relative error

For a Taylor expansion of order 1, GR errors in the boundary elements are reduced, which was found to be sufficient to alter the evolution of those elements in the

particular case considered in Section 3.2.3. Additionally, Taylor expansions of orders higher than 1 may not be appropriate if a non-smooth initial condition is imposed. This is because the elements considered for the gradient reconstruction will not only be stencil points immediately adjacent to the mesh element, but also distant points to those.

3.2.3 Benchmark results in MFA meshes

A comparison between the results using a MFAM (axisymmetric domain) and a structured mesh (for an infinite slab) is possible, due to the fact that, formally, both are considered two-dimensional cases.

The evolution of the solution to the anisotropic diffusion equation in a MFA mesh against a structured mesh is depicted in Figure 3.9. For this particular case, the magnetic field geometry is equal to that generated by current traversing an infinitely large wire perpendicular to the computational domain. The MFA mesh will be formed by lines of constant λ, describing concentric circles centered at the position of the wire, with σ lines perpendicular to them. The problem in the structured, non-aligned mesh has been generalized by locally computing the magnetic field orientation; instead of having straight field lines at an angle α, they can be assumed to have a "variable α" with the grid coordinates.

As it can be observed, the domains are of the same dimensions, having both problems the same initial conditions: equal initial plasma density regions, same diffusion ratio $\Theta = 100$, and a mesh resolution of 1800 elements. The selection of Θ was done attending to Figure 3.11a, as this ratio allows to visualize a larger difference in the solution between both meshes. Notice that the density (n') is adimensionalized with a reference density $n = 1 \cdot 10^{17}\, m^{-3}$.

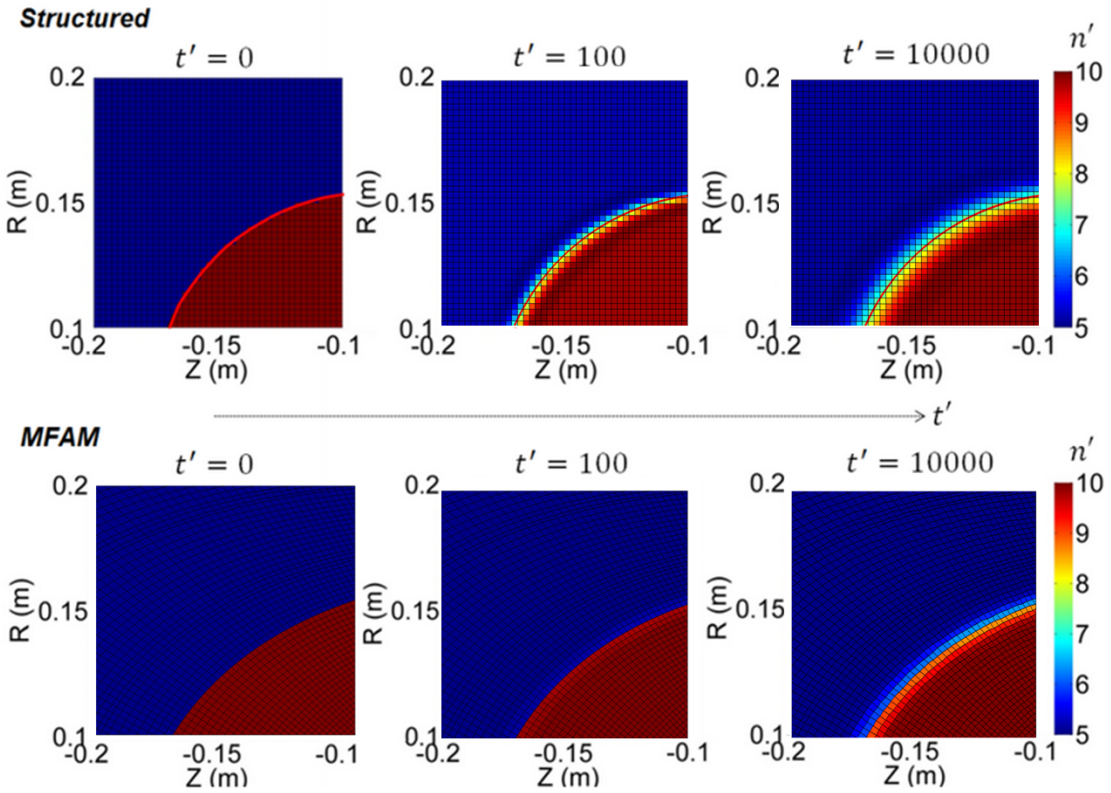

Figure 3.9: Evolution of the system in the structured and MFA meshes

As evidenced by the results, the error committed in the MFAM due to gradient reconstruction and lower quality boundary elements is not comparable to that induced by numerical diffusion, which largely affects the solution in the structured mesh. This is also appreciated in Figure 3.10, where the difference between the solutions of both meshes is compared. Based on it, numerical diffusion does not evenly occur throughout the diffusion region (larger differences are observed in the central part).

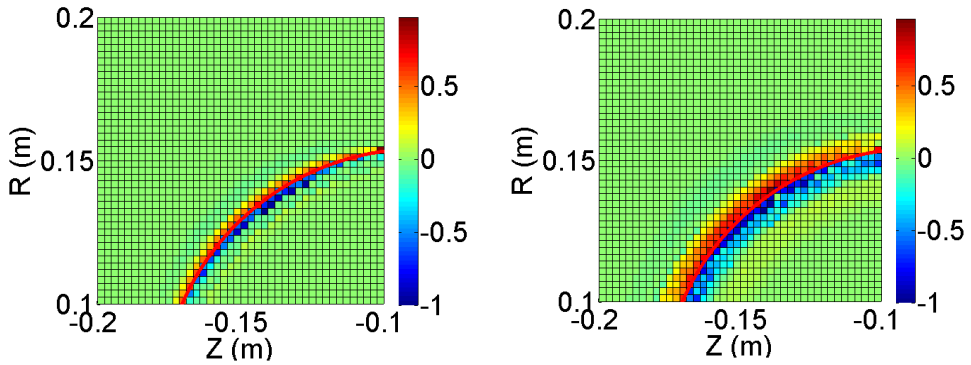

(a) t' = 100 (b) t' = 10,000

Figure 3.10: Normalized differences in the numerical solutions using the structured mesh compared to the MFAM

The evolution of the problem in terms of the adimensionalized average density of the elements located in the initial low density region is also compared in Figure 3.11.

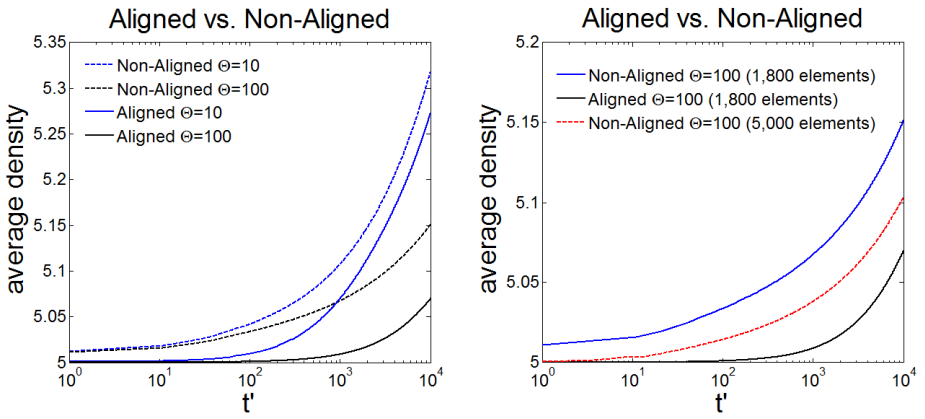

(a) Different diffusion coefficient, Θ (mesh resolution = 1.800 elements)

(b) Different mesh resolution (Θ = 100)

Figure 3.11: Adimensionalized average density evolution for elements at the initial low density region

According to Figure 3.11a, the transfer of mass enhanced by numerical diffusion becomes more evident for highly anisotropic systems. Additionally, and although both solutions will diverge for sufficiently large times, it is necessary to have a much more refined structured mesh if we wish to recover the solution of the MFAM with a less number of elements (Figure 3.11b); which, up to some extent, may be prohibitive from the computational perspective. This outlines the fact that, despite the issues involved, MFA meshes provide with a more correct approach on the modeling of highly anisotropic systems, specially, as we have mentioned before, in those systems in which the anisotropicity level is not known a-priori.

Chapter 4

Conclusions

The study carried out in this bachelor thesis has provided insight in the errors arising when solving the anisotropic plasma diffusion equation in structured, non-aligned meshes, as well as a benchmark against the solution of a highly anisotropic problem using a non-structured MFA mesh.

Specifically, numerical diffusion is due to the highly anisotropic nature of a magnetized plasma, and appears when projecting the diffusion term onto the local coordinate system of a computational grid unaligned with the magnetic field. There are two effects that may be derived from the projected diffusion term: first, the cross-terms induce an undesirable transfer of mass along the facets of the mesh elements (i.e.: between the facet nodes). Second, as the simulation progresses, mass also appears to diffuse across the element facets at a higher rate than should be allowed by the physical diffusion mechanism.

The evolution of a highly anisotropic problem ($\Theta \to \infty$) in a structured mesh has shown that numerical diffusion will largely affect the solution, which has been quantified through an average error. In fact, it is concluded that lower degrees of anisotropicity may lead to better results since the errors are partially contained as mesh resolution is increased; in fact, no error would appear if the diffusion coefficients in the directions perpendicular and parallel to the magnetic field are equal (i.e.: in the non-anisotropic limit). Furthermore, by means of a qualitative analysis, numerical diffusion has been proved to remain fairly constant for different degrees of misalignment.

Geometric mesh quality has been assessed using three different meshes: Regular, Random and Gaussian. It is concluded that mesh quality in structured meshes is unlikely to affect numerical diffusion; the evolution of the average error is of the same order for all of the explored meshes.

The evolution of a highly anisotropic problem in a structured mesh has been

compared against the solution using a non-aligned MFAM. In spite of the errors present in the later, which may arise from gradient reconstruction methods and mesh irregularities, but are not due to numerical diffusion, MFA meshes provide with a more correct approach to solving highly anisitropic problems in magnetized plasma simulations.

As an additional conclusion, we suggest that it might be reasonable to consider the use of non-aligned meshes for smaller anisotropicity ratios (if computational resources are able to deal with the required mesh resolution), instead of facing the difficulties present in the building process of MFAMs and the issues regarding a correct handling of the gradient reconstruction method. Notwithstanding, we usually lack of a prior knowledge of the degree of anisotropicity since the complex magnetic field topologies present in electric propulsion devices lead to different regions of confinement within the discharge channel. Therefore, it is concluded that the use of MFAMs on the modeling of highly anisotropic problems or problems of unknown or non-uniform anisotropicity in magnetically confined plasmas (or specific populations inside them) stands out as the best alternative to structured meshes.

4.1 Budget estimation

A preliminary estimation of the budget necessary to accomplish the present project is presented in Table 4.1.

Concept	Units	Unitary cost	Cost
Engineering	600 h	42 €/h	25,200 €
MATLAB®2015 academic license	1	500 €	500 €
Total cost			25,700 €

Table 4.1: Budget estimation

It mainly consists on two items:

- The engineering work, accounted as the total number of hours that have been required for the development of this project. This comprises all the different stages: from the understanding of the problem, to the implementation of the numerical model and analysis of the results.

- The software licensing costs, which correspond to an academic version of the MATLAB®2015 programming platform, as specified in the official website.

4.2 Future work

As evidenced by the results, non-structured MFAMs offer a distinct approach when solving the anisotropic plasma diffusion equation in highly anisotropic systems, compared against structured, non-aligned meshes. However, a more correct approach on the numerical modeling of magnetically confined plasmas may require to consider other physical phenomena that happen during the real operation of certain electric propulsion systems.

Future work may be oriented toward a more realistic comparison between aligned and non-aligned meshes. This would require to account for the transfer of momentum and the exchange of energy among the different species present in the plasma. Indeed, the results arising from this comparison may provide reasonable arguments to address whether efforts should be focused on the development of Magnetic Field-Aligned Meshes. Therefore, seeking for more accurate simulations, giving a deeper insight into the modeling of various EP systems, such as electromagnetic thrusters.

Appendix A

Code validation

To verify the correct implementation of the algorithm, the evolution of several arbitrary volume elements of a randomly generated mesh was compared against the expected results obtained through separate calculations. A detailed analysis for two different sample cases is presented: calculation of the interpolated density at one node, followed by the density evolution in a mesh element. Additionally, because of the selection of an explicit method for time integration (particularly the Euler method), we must asses the stability condition of the numerical scheme to ensure correct integration of our problem.

A.1 Comparison of the results

Considering a problem with $\alpha = 45^{o}$ and $\Theta \to \infty$, Figure A.1 presents the position of the concerned node (left) and element (right) in the mesh, as well as the surrounding elements or nodes involved in the calculations.

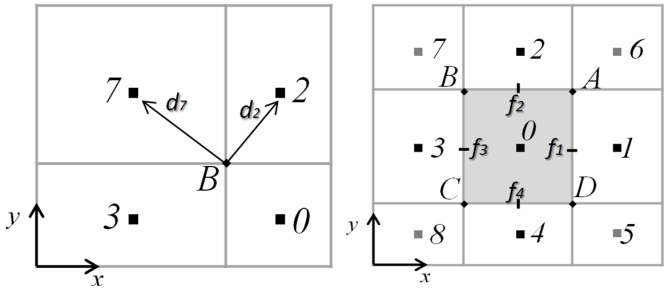

Figure A.1: Definition of the elements and nodes involved in the calculations

A.1.1 Interpolated density at one node

For each node, the interpolated density is calculated as explained in Section 2.2.3: first, a set of coefficients are assigned to the elements surrounding the node according to Equation 2.27, which are then multiplied by the density at each of these stencil points. Finally, all the contributions are summed to obtain the interpolated density at the node. For the node considered in Figure A.1 left (node B), Table A.1 gathers the relevant data of the problem, as well as the calculated value for each of the coefficients, C. Note that n' is adimensionalized with a reference density $n = 1 \cdot 10^{17} m^{-3}$.

$$C_i = \frac{1/d_i}{\sum_{i=1}^{s}(1/d_i)} \qquad \text{(2.27 revisited)}$$

Element	1/d (m^{-1})	n'	C
2	0.0047	4.89	0.2718
7	0.0058	4.80	0.2202
3	0.0057	4.89	0.2241
0	0.0045	5.74	0.2839

Table A.1: Elements information and assigned coefficients

Therefore, the interpolated density at node B is equal to: $\mathbf{n'} = \mathbf{5.11}$, which coincides with the value calculated by the algorithm.

A.1.2 Density evolution in a mesh element

We will compute the fluxes either entering or leaving the element shown in Figure A.1 right (Element 0). For a given $\Delta t = 10^{-5} s$, the change in density of the element can be computed using Equations 2.21 and 2.23 together with the data gathered in Tables A.2, A.3, and A.4. Note that n' is adimensionalized with a reference density $n = 1 \cdot 10^{17} m^{-3}$.

$$V_e \frac{n_{e,i}^{t+\Delta t} - n_{e,i}^{t}}{\Delta t} = \sum_j \left((D \cdot \nabla n)|_{f,j} \cdot dA_{f,j} \cdot \vec{n_{f,j}} \right) \qquad \text{(2.21 revisited)}$$

$$(D \cdot \nabla n)|_{f,j} = \left[\begin{array}{c} (D_\perp \cos^2\alpha + D_\parallel \sin^2\alpha)\frac{\partial n}{\partial x} + ((D_\parallel - D_\perp)\cos\alpha \sin\alpha)\frac{\partial n}{\partial y} \\ ((D_\parallel - D_\perp)\cos\alpha \sin\alpha)\frac{\partial n}{\partial x} + (D_\parallel \cos^2\alpha + D_\perp \sin^2\alpha)\frac{\partial n}{\partial y} \end{array} \right]\Bigg|_{f,j} \qquad \text{(2.23 revisited)}$$

Element	n'	d (m)	$\frac{\partial n}{\partial x}\Big\vert_f (m^{-1})$	$\frac{\partial n}{\partial y}\Big\vert_f (m^{-1})$
1	7.13	0.0063	220.63	-201.37
2	4.89	0.0075	-113.33	129.63
3	4.88	0.0070	122.86	-127.40
4	7.48	0.0074	-235.13	229.63

Table A.2: Elements information. The gradients are calculated at the faces between the element considered and the shaded element (Element 0)

Node	n'
A	5.81
B	5.11
C	6.04
D	7.28

Table A.3: Nodes information

n'	$A_{f2,f4}(m)$	$A_{f1,f3}(m)$	$\vec{n}\vert_{f1}$	$\vec{n}\vert_{f2}$	$\vec{n}\vert_{f3}$	$\vec{n}\vert_{f4}$
5.740	0.0054	0.0073	(1,0)	(0,1)	(-1,0)	(0,-1)

Table A.4: Characteristics of the shaded mesh element (Element 0)

Using a shorter notation for Equation 2.23:

$$D \cdot \nabla n|_{f,j} = \left[\begin{array}{cc} A\frac{\partial n}{\partial x} & B\frac{\partial n}{\partial y} \\ B\frac{\partial n}{\partial x} & C\frac{\partial n}{\partial y} \end{array} \right]\Bigg|_{f,j} \tag{A.1}$$

The flux, Γ_i, entering or leaving the mesh element across faces f_1, f_2, f_3, f_4 is given by:

$$\begin{aligned} \Gamma_i A_f \cdot \vec{n}_f = &\left(A\frac{\partial n}{\partial x}\Big|_1 + B\frac{\partial n}{\partial y}\Big|_1\right) A_1 \cdot \vec{n}_1 \\ &+ \left(B\frac{\partial n}{\partial x}\Big|_2 + C\frac{\partial n}{\partial y}\Big|_2\right) A_2 \cdot \vec{n}_2 \\ &+ \left(A\frac{\partial n}{\partial x}\Big|_3 + B\frac{\partial n}{\partial y}\Big|_3\right) A_3 \cdot \vec{n}_3 \\ &+ \left(B\frac{\partial n}{\partial x}\Big|_4 + C\frac{\partial n}{\partial y}\Big|_4\right) A_4 \cdot \vec{n}_4 \end{aligned} \tag{A.2}$$

Which leads to $\mathbf{n_e^{t+\Delta t} = 5.747}$. We have run the code using the mesh of Figure A.1 and results are in agreement with those obtained here; thus, validating the correct implementation of the algorithm.

A.2 Stability condition

The time step that ensures stability can be determined through a Von Neumann stability analysis. In order to guarantee a stable scheme the numerical method should produce a bounded solution. The stability criteria imposes a limit on the time step, according to which a Δt greater than the maximum allowed will provide divergent results and possibly non-physical, such as negative density. Considering the numerical scheme to be:

$$\begin{aligned} n_{i,j}^{t+\Delta t} =& n_{i,j}^t + \alpha(n_{i+1,j}^t + n_{i-1,j}^t - 2n_{i,j}^t) + \beta(n_{i,j+1}^t + n_{i,j-1}^t - 2n_{i,j}^t) + \\ &+ \gamma(n_{i+\frac{1}{2},j+\frac{1}{2}}^t - n_{i-\frac{1}{2},j+\frac{1}{2}}^t + n_{i-\frac{1}{2},j-\frac{1}{2}} - n_{i+\frac{1}{2},j-\frac{1}{2}}^t) \end{aligned} \tag{A.3}$$

With:

$$\begin{aligned} \alpha &= \frac{\Delta t D_{xx}}{\Delta x^2} \\ \beta &= \frac{\Delta t D_{yy}}{\Delta y^2} \\ \gamma &= \frac{2 D_{xy}}{\Delta x \Delta y} \end{aligned} \tag{A.4}$$

Where D_{xx}, D_{xy} and D_{yy} refer to the components of the diffusion term expressed as in Equation 2.16. If the Δt exceeds the limit imposed by the stability condition, the error (ϵ), defined as the difference between the numerical solution of the discretized equation and the exact solution (which might be obtained by separation of variables), may diverge and dominate the solution. Therefore, the stability condition must ensure that this error will decay as time increases. Because of linearity of the numerical scheme, the error does also satisfy the discretized equation. Any solution of this numerical scheme can be decomposed into a Fourier series, which are solutions of the form:

$$\begin{aligned} n_{i,j}^t &= n^t \, e^{i(ax+by)} \\ \epsilon_{i,j}^t &= \epsilon^t \, e^{i(ax+by)} \end{aligned} \tag{A.5}$$

If Equation A.5 is substituted in Equation A.3, we obtain an expression of the form:

$$\begin{aligned}\frac{\epsilon^{t+\Delta t}}{\epsilon^t} =& 1+\alpha(e^{ia\Delta x}+^{-ia\Delta x}-2)+\beta(e^{ib\Delta y}+e^{-ib\Delta y})+\\ &+\gamma(e^{i(a\frac{\Delta x}{2}+b\frac{\Delta y}{2})}-e^{i(-a\frac{\Delta x}{2}+b\frac{\Delta y}{2})}+e^{-i(a\frac{\Delta x}{2}+b\frac{\Delta y}{2})}-e^{-i(-a\frac{\Delta x}{2}+b\frac{\Delta y}{2})})\end{aligned} \tag{A.6}$$

The left-hand side of Equation A.6 is called the amplification factor. The necessary condition for the error to remain bounded is that:

$$\left|\frac{\epsilon^{t+\Delta t}}{\epsilon^t}\right| \leq 1 \tag{A.7}$$

Which states that the difference between the solution of the numerical scheme and the exact solution should not increase after a time step. Imposing the stability condition in Equation A.6, and using the identities:

$$\begin{aligned}\sin^2\left(\frac{\phi}{2}\right) &= \frac{1-\cos(\phi)}{2}\\ \cos(\phi) &= \frac{e^{i\phi}+e^{-i\phi}}{2}\end{aligned} \tag{A.8}$$

Equation A.6 can be written as:

$$\begin{aligned}1 \geq \Bigg|1 &- 4\alpha\sin^2\left(\frac{a\Delta x}{2}\right)-4\beta\sin^2\left(\frac{b\Delta y}{2}\right)-4\gamma\sin^2\left(\frac{a\frac{\Delta x}{2}+b\frac{\Delta y}{2}}{2}\right)\\ &-4\gamma\sin^2\left(\frac{-a\frac{\Delta x}{2}+b\frac{\Delta y}{2}}{2}\right)\Bigg|\end{aligned} \tag{A.9}$$

It might be proved that we reach the following stability condition: $\alpha+\beta+\gamma \leq \frac{1}{2}$. This relation imposes a limit on the time step equal to:

$$\Delta t \leq \frac{\Delta x^2\Delta y^2}{2(D_{xx}\Delta y^2+D_{yy}\Delta x^2+2D_{xy}\Delta x\Delta y)} \tag{A.10}$$

As it is shown, the restrictions on Δt are given by both, the mesh refinement and the diffusion terms.

Appendix B

Conference paper on numerical diffusion

This annex includes a conference paper on numerical diffusion, in which part of the results of this Bachelor Thesis have been included.

Benchmarks for Magnetic Field Aligned Meshes in Electromagnetic Plasma Thruster Simulations

IEPC-2015-203/ISTS-2015-b-203

Presented at Joint Conference of 30th International Symposium on Space Technology and Science, 34th International Electric Propulsion Conference and 6th Nano-satellite Symposium
Hyogo-Kobe, Japan
July 4–10, 2015

D. Pérez-Grande*, O. Gonzalez-Martinez, P. Fajardo and E. Ahedo†
Aerospace Engineering Group, Universidad Carlos III de Madrid, Spain

Keywords: Plasma Propulsion, Magnetic Field Aligned Mesh, Numerical Diffusion, Benchmarks

A short study on numerical errors for highly anisotropic diffusion problems in propulsion plasmas is presented in order to address the use of magnetic field aligned meshes versus regular structured meshes in numerical solutions. Numerical diffusion in structured meshes is quantified by solving the classical anisotropic diffusion problem. Meshing strategies and Gradient Reconstruction methods for magnetically aligned meshes are presented in order to provide insight into achieving acceptable mesh regularity. Numerical errors are compared for a benchmark problem on structured and magnetically aligned meshes. It is concluded that the latter provides a more correct approach to solving problems with anisotropicity, specially if anisotropicity levels are high or difficult to quantify.

I. Introduction

A typical assumption in the modeling of *electric propulsion plasmas* is that the electron population (which is generally the only one "magnetized", i.e., confined by the magnetic field) can be considered a maxwellian fluid of a highly anisotropic nature, in which transport in the perpendicular and parallel directions to the magnetic field is widely different. The equations which govern the evolution of the electron population can be solved in a curvilinear system of coordinates defined through the local magnetic field directions, as long as the magnetic field may be considered "static" (i.e., the magnetic field $\vec{B}$ can be assumed irrotational in addition to solenoidal and stationary); the numerical simulation mesh whose element facets are locally aligned with the magnetic field directions is called the Magnetic Field Aligned Mesh (MFAM), as shown in Fig. 1.

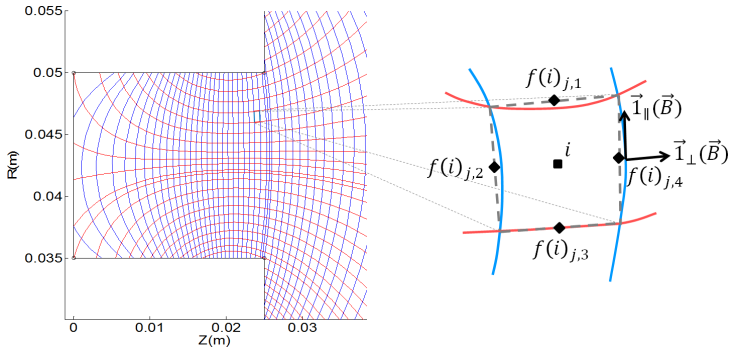

Figure 1. MFAM in an axisymmetric simulation domain for the SPT-100 HET & *detail* of Mesh element

*Correspondence Author @ daperezg@ing.uc3m.es
†Keynote Speaker

An added perk to discretizing the problem on the MFAM is that this approach helps to avoid "artificial" numerical diffusion plaguing the solution; indeed, because of the large anisotropicity in the electron transport coefficients for the parallel and perpendicular directions, solving the governing equations in a mesh which is *not* aligned with the magnetic field may lead to "cross-contamination" of the transport coefficients and thus to numerical diffusion (please refer to Section II). The MFAM venue has been utilized extensively both by the fusion plasma[1] and the plasma propulsion[2] communities, and numerical diffusion has been documented in simulations for highly anisotropic systems;[3,4] however, a number of difficulties may arise when using the MFAM, mainly in relation to low quality meshes, problematic boundary elements, calculation of gradients and the errors associated with them, as discussed by Araki.[5]

The EP2 Group[a] at UC3M, building from the expertise gained from the development of the HPHall-2 and HallMA codes,[6] is currently developing NOMADS (NOn-structured Magnetically Aligned plasma Discharge Simulation), an advanced platform for simulation of plasma discharges in various thruster configurations and magnetic field topologies. Specifically, NOMADS is aimed at solving plasma discharges in Hall Effect Thrusters -HETs- and derived HETs with non-regular magnetic field topologies: singular points, cusp regions, etc. For this, the electron population will be modeled as a bi-Maxwellian (non-isotropic Velocity Distribution Function), magnetized, fluid, and solved in the MFAM.

Following the discussion by Araki,[5] efforts have been carried out to justify using the MFAM as opposed to regular, structured, meshes. The present work tackles the issues of numerical diffusion in regular meshes and mesh quality and gradient reconstruction issues in non-structured meshes; additionally, a *benchmark* test is presented showcasing the benefits of using MFAMs versus structured meshes in anisotropic problems.

II. Numerical Diffusion in regular, structured, meshes: the anisotropic diffusion problem

The classical *anisotropic diffusion problem* in magnetized plasmas is well known: it is similar to the *ambipolar diffusion problem* (in which an ambipolar electric field is established to balance the fluxes of the electron and ion species), except that the parallel ($\parallel$) and perpendicular ($\perp$) transport coefficients account for the anisotropy of the problem and currents flowing in the direction of the magnetic field are responsible for space charge neutrality.

A formal derivation by Simon,[7] considering the quasineutrality $n_e \approx n_i = n$ assumption, for an infinite 2D slab with conducting walls under a straight magnetic field leads to Eq. (1):

$$\frac{dn}{dt} = \begin{bmatrix} \frac{\mu_e D_{i\perp} - \mu_i D_{e\perp}}{\mu_e - \mu_i} & 0 \\ 0 & \frac{\mu_e D_{i\parallel} - \mu_i D_{e\parallel}}{\mu_e - \mu_i} \end{bmatrix} \begin{bmatrix} \frac{\partial^2 n}{\partial x'^2} \\ \frac{\partial^2 n}{\partial y'^2} \end{bmatrix} \tag{1}$$

Where the μ terms are the mobility coefficients for both species and $D_\perp$ and $D_\parallel$ are, respectively, the diffusion across the magnetic field (which only accounts for classical collision mechanisms) and the "free" or natural diffusion coefficient (which appears in the non-confined direction parallel to the magnetic field); x' and y' are, respectively, the coordinates associated to the directions perpendicular ($\vec{1}_\perp$) and parallel ($\vec{1}_\parallel$) to the magnetic field.

For the sake of simplicity, we neglect the effects of the ambipolar perpendicular electric field for non-conducting walls and consider that the Diffusion term is uniform across the plasma, and simply defined as:

$$\mathcal{D}' = \begin{bmatrix} D_\perp & 0 \\ 0 & D_\parallel \end{bmatrix} ; \Theta = \frac{D_\parallel}{D_\perp} \tag{2}$$

Where Θ is the *diffusion coefficient ratio* and is the main parameter in this study, as it will determine the rate of numerical diffusion. Formally, this equation may be expressed in the way of the classical diffusion equation, taking into account the flux vector Γ and strictly positive diffusion coefficients, as:

$$\frac{dn}{dt} = \nabla' \cdot \left[\mathcal{D}' \cdot \nabla' n \right] = \nabla' \cdot \vec{\Gamma'} = \nabla' \cdot \begin{bmatrix} \Gamma_{x'} \\ \Gamma_{y'} \end{bmatrix} \tag{3}$$

[a] http://aero.uc3m.es/ep2/

The numerical diffusion problem arises when the diffusion equation (Eq. (3)) is discretized in a coordinate system which is not aligned with the perpendicular and parallel directions of the magnetic field, such as a cartesian coordinate system for a randomly aligned magnetic field (Fig. 2). For simplicity we will consider that magnetic field lines are straight (although the problem is generalizable to a "curved" field) and that the magnetic versors ($\vec{1}_\perp$, $\vec{1}_\parallel$) are rotated an angle α with respect to the cartesian system.

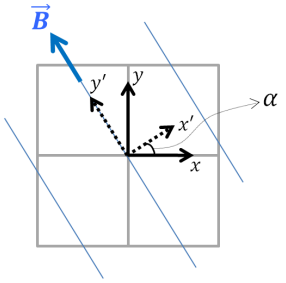

Figure 2. Regular structured mesh with angled Magnetic field

The rotation matrix $\mathcal{R}$ allows allows for transforming Eq. (3) into cartesian coordinates by using the relations:

$$\mathcal{R} = \begin{bmatrix} \cos\alpha & -\sin\alpha \\ \sin\alpha & \cos\alpha \end{bmatrix}; \vec{\Gamma} = \mathcal{R} \cdot \vec{\Gamma'}; \nabla' n = \mathcal{R} \cdot \nabla n \tag{4}$$

Which results in a diffusion equation in cartesian coordinates which satisfies:

$$\frac{dn}{dt} = \nabla \cdot \left[\mathcal{R}^{-1} \mathcal{D}' \mathcal{R} \cdot \nabla n \right]; \tag{5}$$

$$\mathcal{D} = \mathcal{R}^{-1} \mathcal{D}' \mathcal{R} = \begin{bmatrix} D_\perp \cos^2\alpha + D_\parallel \sin^2\alpha & \left(D_\parallel - D_\perp\right) \cos\alpha \sin\alpha \\ \left(D_\parallel - D_\perp\right) \cos\alpha \sin\alpha & D_\parallel \cos^2\alpha + D_\perp \sin^2\alpha \end{bmatrix}$$

Integrating over each mesh element volume and applying the Gauss divergence theorem in Eq. (5) we reach an expression which must be satisfied for every mesh element:

$$\int_V \frac{dn}{dt} = \oint_A \begin{bmatrix} (D_\perp \cos^2\alpha + D_\parallel \sin^2\alpha) \frac{\partial n}{\partial x} + \left(\left(D_\parallel - D_\perp\right) \cos\alpha \sin\alpha) \frac{\partial n}{\partial y} \right) \\ \left(\left(D_\parallel - D_\perp\right) \cos\alpha \sin\alpha) \frac{\partial n}{\partial x} \right) + (D_\parallel \cos^2\alpha + D_\perp \sin^2\alpha) \frac{\partial n}{\partial y} \end{bmatrix} \cdot d\vec{A} \tag{6}$$

Equation (6) is analogous to the one derived by Wirz[8] and demonstrates how numerical diffusion appears in non-aligned meshes. Indeed, the Diffusion term expressed in cartesian coordinates will be responsible for the "cross-contamination" we mentioned earlier, due to the fact that, in general, $D_\parallel \gg D_\perp$; numerical diffusion appears even when the diffusion coefficient ratio is $\Theta \to \infty$ ($D_\perp = 0$), the plasma is perfectly confined), this may be simply understood through the sketch in Fig. 3: first, the cross-diffusion term induces a transfer of mass between contiguous cells when none should occur (Fig. 3a)); second, for $\Theta \to \infty$ magnetic field lines are impermeable to mass-flow, and yet, because of the iterative nature of numerical solutions, mass will "creep" through the mesh cells (Fig. 3b)) due to the lack of alignment between the mesh and the magnetic field.

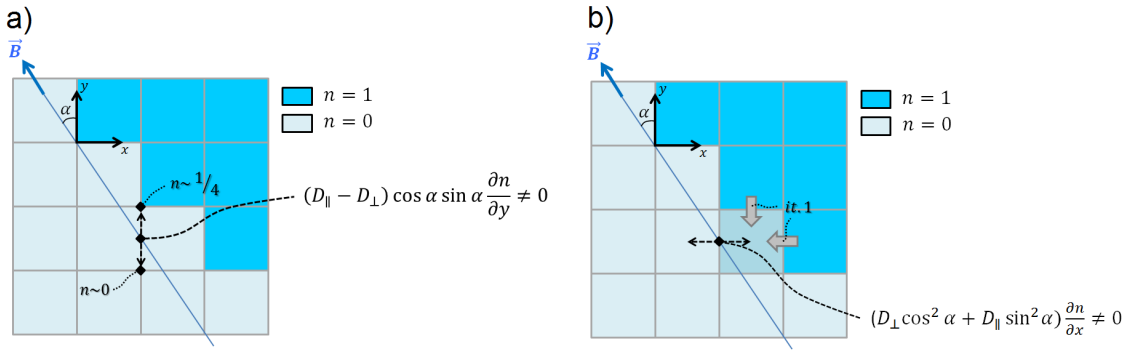

Figure 3. Sketch on numerical diffusion

A. Case Results

Equation (6) may be solved using the Finite Volume Method (FVM), which is also utilized in NOMADS, as it provides a formulation of the problem in conservative form (versus the weak forms of the Finite Element and Finite Differences Methods); for a particular mesh volume element, this equation is discretized for each element by an *explicit Euler method* as:

$$V_i \frac{n_{e,i}^{t+\triangle t} - n_{e,i}^{t}}{\triangle t} = \\ = \sum_j \left(\left[\begin{array}{l} (D_\perp \cos^2\alpha + D_\parallel \sin^2\alpha)\frac{\partial n}{\partial x} + \left((D_\parallel - D_\perp)\cos\alpha\sin\alpha\right)\frac{\partial n}{\partial y} \\ \left((D_\parallel - D_\perp)\cos\alpha\sin\alpha\right)\frac{\partial n}{\partial x} + (D_\parallel \cos^2\alpha + D_\perp \sin^2\alpha)\frac{\partial n}{\partial y} \end{array} \right] \Bigg|_{f,j} \cdot dA_{f,j}\vec{n}_{f,j} \right) \tag{7}$$

Where "e, i" represents the i^{th} *element* and "f, j" the j^{th} facet of that element. Derivatives on the regular structured mesh are approximated by a central differencing scheme (in the same way as shown in Ref. 8), based on the sketch in Fig. 4 as:

$$\frac{\partial n}{\partial x} \approx \frac{n_2 - n_1}{\triangle x}; \frac{\partial n}{\partial y} \approx \frac{\frac{n_1+n_2+n_3+n_4}{4} - \frac{n_1+n_2+n_5+n_6}{4}}{\triangle y} \tag{8}$$

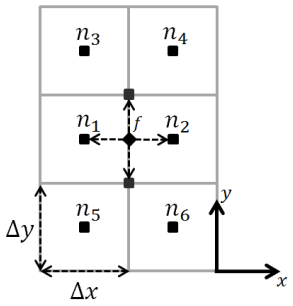

Figure 4. Central Differences schematic

Equation (7) is applied to each element leading to a system of equations contained in a sparse matrix; we may use numerical solvers to obtain the evolution of the anisotropic diffusion problem (with $\Theta = {}^{D_\parallel}/_{D_\perp}$) for the "less-formal" *non-permeable walls* under a magnetic field forming an angle α with the cartesian system. Fig. 5 shows the system evolution for $\alpha = -45°$ and $\Theta \to \infty$ which, as expected, presents numerical diffusion (the *red line* in the figure represents a magnetic field line and as such should be impermeable to the plasma given the initial conditions).

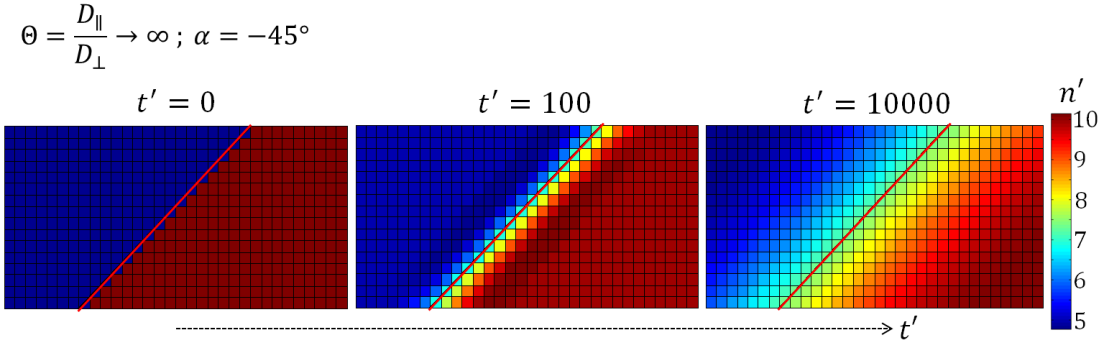

Figure 5. Numerical Diffusion in anisotropic diffusion problem (variables are non-dimensional)

Errors committed due to numerical diffusion for the with $\Theta \to \infty$ case with different α and different number of mesh elements are quantified through the average error density for the elements in the "low density" zone (left of the red line in Fig. 5), considering that the plasma should be perfectly confined:

$$\langle error(t) \rangle = \frac{1}{N_{elem}} \sum_{i=1}^{N} \frac{|n_i(t) - n(t=0)|}{n(t=0)} \tag{9}$$

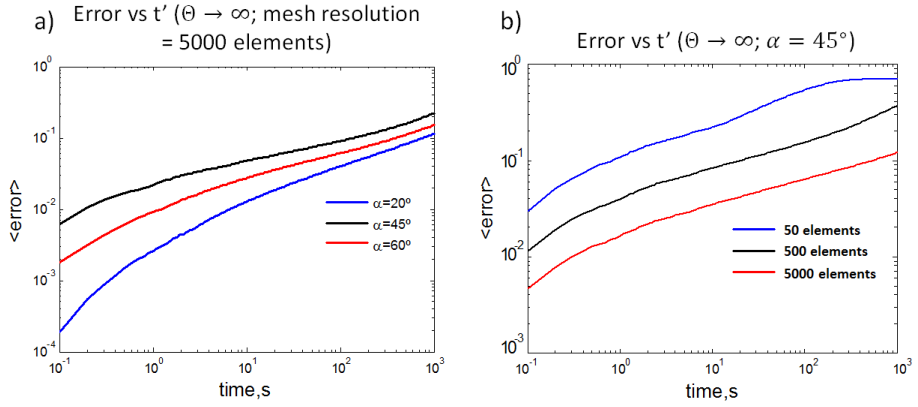

Figure 6. a) Error vs. t' for different α; b) Error vs. t' for different mesh resolution

Figure 6 quantitatively shows the evolution of the error due to numerical diffusion in our problem; however, we wish to seek a more qualitative result in order to assess the effects of numerical diffusion. For this reason we propose the concept of *effective diffusion coefficient ratio* Θ_{eff}: for a given simulation domain, mesh resolution, number of elements in the initial low/high plasma density regions, α and Θ, we study an analogous problem in which the mesh and magnetic fields are aligned; the $\Theta_{"aligned"}$ for the "aligned" mesh which provides an equivalent *diffusive mass flux* (between the different plasma density regions) to the "non-aligned" problem is the Θ_{eff}.

	$\Theta_{eff} \sim ...$	$\Theta \to \infty$	$\Theta = 100$	$\Theta = 10$
Mesh resolution = 50 elements	$\alpha = 20^o$	~ 5	~ 4	~ 3
	$\alpha = 45^o$	~ 5	~ 5	~ 3
	$\alpha = 60^o$	~ 5	~ 5	~ 3
Mesh resolution = 500 elements	$\alpha = 20^o$	~ 20	~ 15	~ 5
	$\alpha = 45^o$	~ 25	~ 15	~ 5
	$\alpha = 60^o$	~ 20	~ 15	~ 6
Mesh resolution = 5000 elements	$\alpha = 20^o$	~ 50	~ 25	~ 8
	$\alpha = 45^o$	~ 50	~ 30	~ 8
	$\alpha = 60^o$	~ 50	~ 30	~ 7

Table 1. ***Effective Diffusion Coefficient ratio*** **(Θ_{eff}) for different mesh resolutions, alignment of the magnetic field (α) and diffusion coefficient ratios (Θ)**

Table 1 presents results for the effective diffusion coefficient with different parameter sets for the problem described by Eq. (6), solved through an explicit Euler/FVM discretization. Results are in line with both Ref. 3 and Ref. 4: numerical diffusion leads to a reduction in the anisotropicity of the system, errors are more or less independent to the misalignment of the magnetic field to the mesh (for the explored sets); they are however very noticeable for lower resolution meshes and only partially recoverable through refinement for the high anisotropicity cases.

III. Meshing strategies for MFAMs

A stationary MFAM may be built when the magnetic field in the simulated domain can be considered to be both irrotational ($\nabla \times \vec{B} \approx 0$) as well as solenoidal ($\nabla \cdot \vec{B} = 0$) and stationary ($\frac{\partial \vec{B}}{\partial t} = 0$). Indeed, the irrotational approximation is valid whenever the effect of the plasma discharge over the magnetic field is small compared to the field generated by the magnetic circuit.

The above relations allow us to derive the magnetic stream-line function λ and the magnetic potential function σ, which can be integrated in a typical *axisymmetric* simulation domain (Fig. 7) to obtain a curvilinear system of "magnetic" coordinates:

$$\nabla \cdot \vec{B} = 0 \to \nabla^2 \lambda = 0 \to \frac{\partial \lambda}{\partial r} = -rB_z; \frac{\partial \lambda}{\partial z} = rB_r \tag{10}$$

$$\nabla \times \vec{B} \approx 0 \to \nabla \sigma = \vec{B} \to \frac{\partial \sigma}{\partial r} = B_r; \frac{\partial \sigma}{\partial z} = B_z \tag{11}$$

Lines of constant λ always follow the local direction of the magnetic field ($\vec{1}_{\parallel}$) and lines of constant σ are always in the perpendicular direction to the magnetic field ($\vec{1}_{\perp}$); it is precisely these "isolines" through which we define the non-structured MFAM.

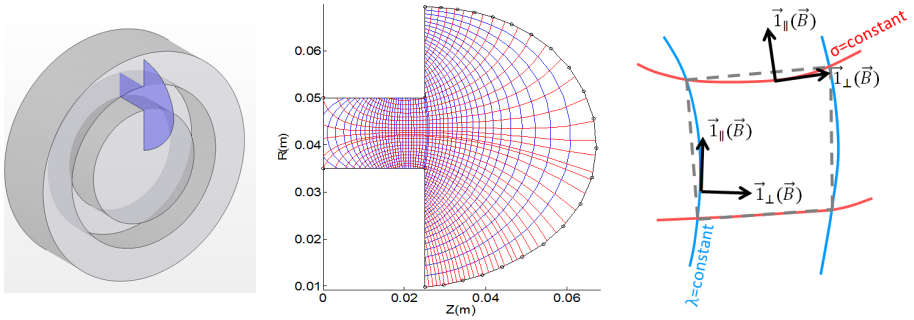

Figure 7. Simulation domain in an SPT-100 HET, Isoline mesh (MFAM) for the SPT-100 magnetic topology (axisymmetric domain) & detail of mesh element

The solution to a highly anisotropic problem posed in the local versor system defined by the magnetic field, with respect to the magnetic coordinates cannot, by definition, show numerical diffusion as understood here (as it would be the equivalent of solving the problem defined by Eq. (1)); however, building a robust mesh in which to solve the problem presents a number of challenges which need to be assessed through different strategies and functionality in the meshing algorithm.

Specifically, issues arise regarding mesh quality, mainly at the domain boundaries; Araki[5] tackles these by sacrificing the MFAM configuration in the boundary elements (and in the elements adjacent to those), choosing to relocate node positions to improve quality. The argument here is that poor mesh quality in the MFAM boundaries leads to errors in the numerical solution which are, at least, comparable to numerical diffusion.

This discussion is reserved for Section V, however, focusing on improvement of mesh quality, correct handling of gradient reconstruction and the implementation of a conservative method, such as the FVM, should allow us to correctly make use of the MFAM across the domain and contain the issue of numerical diffusion with little error specific to the non-structured mesh.

A. Meshing algorithms

A working Mesh Generator, has been built for the NOMADS platform. It performs the following tasks:

- Obtains the magnetic field in the selected simulation domain
- Integrates λ and σ in the domain (this is done over an initial structured cartesian "dummy" mesh)
- Selects λ and σ isolines (contour levels)
- Corrects isolines if required
- Builds the MFAM using the selected isolines; mesh information is stored by elements, facets, nodes, etc.

Two main concerns arise when building the MFAM: first, as the magnetic field is not constant in the domain, picking the contour levels of λ and σ to ensure that lines are correctly spaced requires careful consideration; this is specially true whenever singular points ($\left|\vec{B}\right| = 0$) or local minima appear in the domain: because of low magnetic field strength, there is a smaller variation of λ and σ values around these regions than there is in regions of high magnetic field strength, thus dedicated contour levels must be added in order to avoid excessively large mesh elements. Second, the mesh is determined by the topology of the magnetic field, with the user only being able to "adjust" which contour levels are picked, this implies that we have little control over where the isolines will intersect with the domain boundaries, leading to *low quality boundary elements*.

1. *Contour level initial selection*

The user starts by selecting the number of contour levels of λ and σ which will populate the simulation domain. The Mesh Generator then uses one of various algorithms in order to generate correctly spaced isolines in the mesh (picking specific contour level values), these allow the user to explore the best meshing methodology for the particular problem at hand. The algorithms, or "spacing methods", implemented are:

Smoothing The values for λ and σ are sorted and smoothed using a local regression method which applies weighted least squares and 2nd degree polynomial models; we obtain a correlation between the magnetic coordinate value and the "number" of instances it appears in the domain. We then evenly distribute the number of contour levels selected by the user over the correlation, which provides us with contour level values with a good spatial distribution, independent of the local rate of variation of the magnetic coordinate:

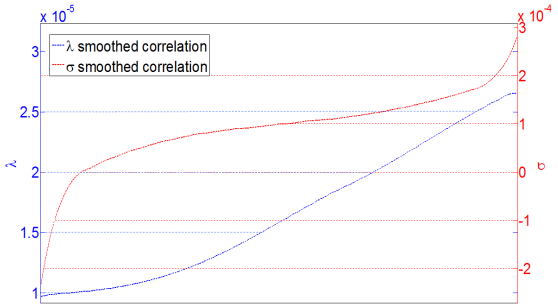

Figure 8. Evenly distributed contour levels based on λ& σ correlations

Logarithmic Obtains logarithmically spaced values for the magnetic coordinate between the maximum and minimum values resulting from the integration; this biases the selection of contour levels toward smaller values (associated with regions of lower magnetic field intensity), avoiding incorrect spacing around high magnetic field intensity regions.

Exponential-stretching This method was proposed by Araki[5] to deal with magnetic field topologies which contained singular regions and/or high ratios of maximum to minimum field strength. For either of the magnetic coordinates (characterized here as ψ), the n_ψ contour levels are obtained from:

$$\begin{cases} \psi_q = \psi_{min} \frac{\exp\left(\frac{q_0-q}{q_0-1}\alpha_\psi\right)-1}{\exp(\alpha_\psi)-1} \text{ for } q < q_0 \\ \psi_q = \psi_{max} \frac{\exp\left(\frac{q-q_0}{n_\psi-q_0}\alpha_\psi\right)-1}{\exp(\alpha_\psi)-1} \text{ for } q > q_0 \\ q_0 = int\left(n_\psi \frac{\psi_{min}}{\psi_{max}-\psi_{min}}\right); \psi(q_0) = 0 \end{cases} \tag{12}$$

which implies obtaining the contour levels by exponentially stretching from $\psi = 0$ to positive and negative values of the magnetic coordinate; α_ψ is the "stretching parameter", which is specified as an input.

"Expanded"-exponential-stretching Based on Araki's method but with an expanded functionality to account for the possibility of having multiple singular points; also allows for specific control of the stretching method around these points (including adding "fractional" levels for fine tuning of the mesh elements and incorporating the contour lines which cross the singular points).

Examples of the meshing algorithms for a typical HET magnetic field the simulation domain are shown in Fig. 9; the method proposed by *Araki* was found to *be consistently more robust in achieving initial meshes with good spacing properties* for the particular magnetic topologies put to trial.

2. Contour level manual correction

However the initial selection of λ and σ isolines is performed, the mesh will present issues with regards to spacing and boundary elements; in case of the latter, issues come in the form of elements with a variable number of facets (three, four, or five), in comparison to interior elements which are always four-sided, the appearance of some small area elements, elements with large aspect ratios (where the boundary facet is very small compared to the others), etc. (refer to Fig. 10)

In order to improve the quality of the MFAM, and also to provide a tool for fine tuning of the mesh, further functionality has been implemented into the Mesh Generator in order to "manually" correct λ and σ isolines; a Graphical User Interface which allows for manually deleting and adding isolines from the simulation domain.

IV. Mesh Regularity: Geometric Quality and Gradient Reconstruction in MFAMs

Recent studies on the effects of "mesh regularity", such as the one performed by Diskin,[9] indicate that the quality of the mesh cannot be truly assessed without taking into account the nature of the problem, the

numerical discretization approach and the expected computational output, in addition to purely geometric quality indicators. Particularly, the FVM method is referred to by Diskin[9] as being *resilient* against the effects of "non-regularity" in non-structured meshes, which provides an additional level of confidence for the argument of utilizing the MFAM approach.

We discuss here results for MFAM quality (geometric and gradient based) without delving into their effects over a particular problem. The understanding is that, however resilient, errors in terms of discretization, interpolation and gradient calculation (which can be linked both to geometric properties of the mesh and to the methods used for gradient reconstruction) may plague our solution; therefore it is best to minimize these issues from the start.

A. Geometric Mesh Quality

The different possibilities offered by the meshing algorithms and the fine tuning through *manual correction* allow the user to iterate through MFAMs with increasingly better geometric quality properties; non withstanding, high quality meshes will always be difficult to achieve due to the restriction of using isolines which are defined by the magnetic topology over "arbitrary" simulation domains.

Qualitatively, geometric quality is described through the following set of element properties:

$$\begin{aligned} smoothness &= \frac{max(A_{element}, A_{adjacent})}{min(A_{element}, A_{adjacent})} \\ aspect\ ratio &= \frac{max(facet{-}length_{element})}{min(facet{-}length_{element})} \\ skewness &= max\left[\frac{\theta_{max}-\theta_e}{180ï¿œ-\theta_e}, \frac{\theta_e-\theta_{max}}{\theta_e}\right] \end{aligned} \tag{13}$$

Where A represents the areas, *element* and *adjacent* represent, respectively, the element being considered and the elements adjacent to it, θ_{max} is the largest angle in the element polygon and θ_e is the angle in an equiangular polygon with the same number of sides as the element considered.

Large aspect ratios and smoothness may be intuitively understood to affect the interpolation of the solution and gradient reconstruction in the element faces (although this may be offset in part by using a "weighted" Least Squares (LSQR) method, see Section IV.B); skewness may be related to large errors for fluxes in facets which are nearly parallel.

In order to showcase how the functionality in the Mesh Generator allows us to improve the geometric quality of the MFAM, we compare two meshes through their quality statistics: one generated using the *smoothing* method with no manual correction and one generated using the *exponential stretching* method and manual correction of the mesh (Fig. 9). Figure 10 shows that we are able to partially recover better geometric quality properties in the mesh through the implemented functionality.

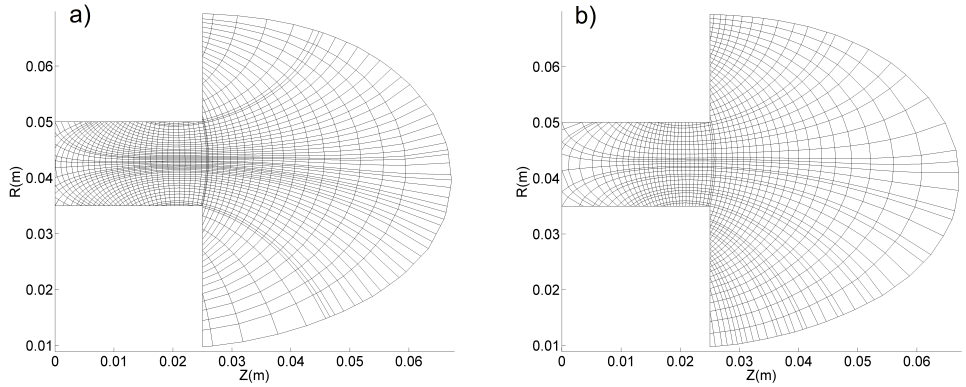

Figure 9. a) Smoothing method (no manual correction); b) Exponential Stretching method & manual correction (initial number of λ and σ isolines = 50)

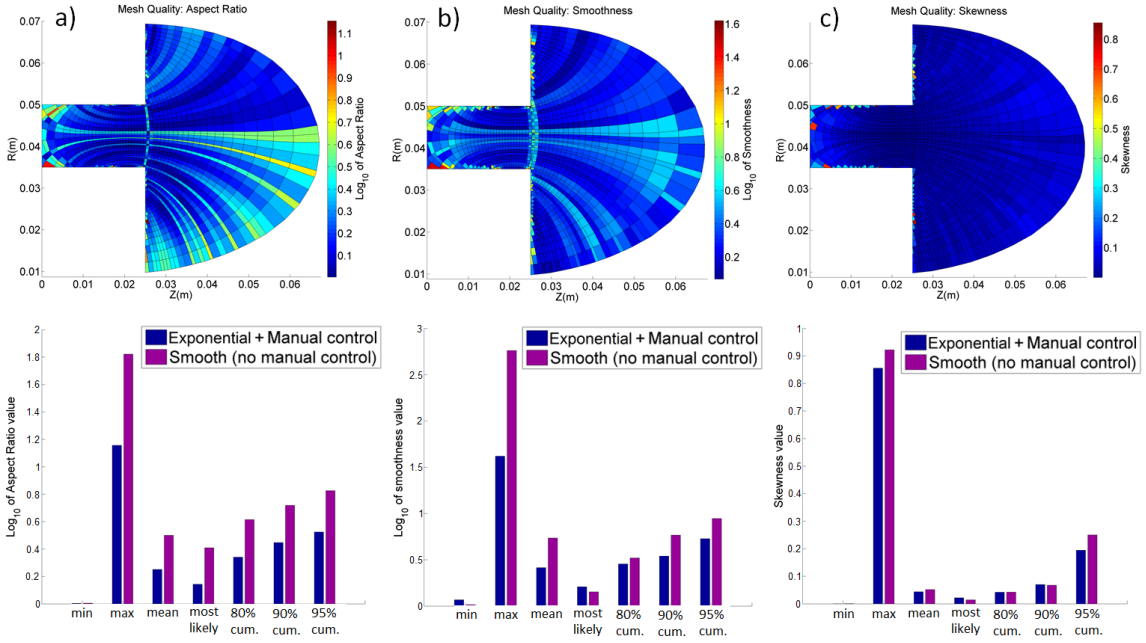

Figure 10. a) Aspect Ratios, b) Smoothness, c) Skewness; (top) 2D profiles in the mesh, (bottom) Comparison for mesh quality statistics between Exponential-Stretching method mesh and Smoothing method mesh -min., max., mean, most likely, 80% cumulative, 90% cumulative, 95% cumulative-

B. Gradient Reconstruction

Gradient reconstruction (GR) is required in "cell-centered" ("element-centered") FVM schemes in order to obtain partial derivatives at the element facets. For regular structured meshes, such as the one employed in Section II.A, central or upwind differencing schemes retain an acceptable order of accuracy; however, whenever dealing with non-structured meshes, such as the MFAM, higher order differencing schemes become necessary.

Both Diskin[9] and Sozer[10] review the use of the Green-Gauss (GG) and the LSQR (both Weighted -WLSQR- and Unweighted -ULSQR-) methods in terms of order of accuracy for GR; Sozer also performs analysis on additional methods, showcasing that, while consistency in the GG and LSQR methods might vary with mesh regularity, other methods tend to have lower orders of accuracy.

We have chosen the WLSQR method for GR in the MFAM; particularly, we use an equivalent to the WLSQR Face Interpolation -WLSQRFI- method described by Sozer[10] as "cell-centered" FVM discretization usually requires gradients at the element facets. The resulting set of equations (based on the Taylor series expansion) determine the value of any function ϕ at the facet center, as well as derivatives and cross-derivatives, from the value of ϕ at a number of *stencil points* and the set of *weights* assigned to them; stencil points are chosen as the centers of the surrounding elements and weights are typically functions of the inverse distance, element areas, etc. (or simply equal to 1 if we wish to recover the ULSQR).

The WLSQR method offers a high level of flexibility to "tune" the quality of GR in a particular mesh: we may choose both the appropriate weights and order of the Taylor series (which can be *done independently for interior and boundary elements in the MFAM*[b], as part of the functionality implemented in our platform).

The main set-back is that we do not know, a-priori, the shape of the function ϕ. We will show that the accuracy of GR depends greatly on both the particular type of function and on the selection of the parameters which confer the flexibility to the method; Fig. 11 shows errors committed by numerical GR, using *inverse-distance weighting* for *Taylor series expansion up to 2nd order (9 stencil points)*, in the "exponential-stretching" mesh (Fig. 9b)) for the following analytical trial functions:

[b] Allowing for a sort of "hybrid mesh", which, as concluded by Sozer,[10] might offer the best compromise between GR methods.

$$\begin{aligned}\phi_1 \sim &\quad \lambda^2 + \sigma^2 \\ \phi_2 \sim &\quad \lambda^3 \cdot \sigma^3 \\ \phi_3 \sim &\quad \sin\lambda \cdot \cos\sigma\end{aligned}$$

Where λ and σ are the magnetic coordinates defined in Eq. (10) and (11). Figure 12 shows variation in error statistics for different weights and Taylor expansion orders for the different trial functions.

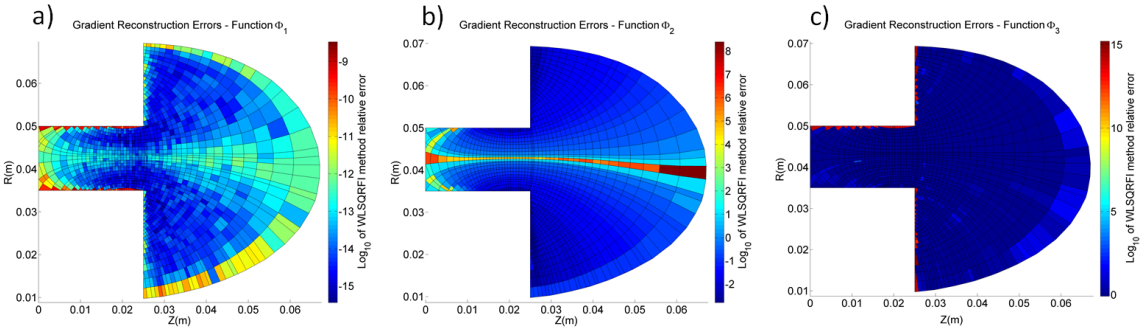

Figure 11. $\log_{10}$ **of relative errors in the WLSQR method -9 stencil points, inverse-distance weighting for a)** ϕ_1**; b)** ϕ_2**; c)** ϕ_3 **(elements are colored according to the worst GR error for their respective facets)**

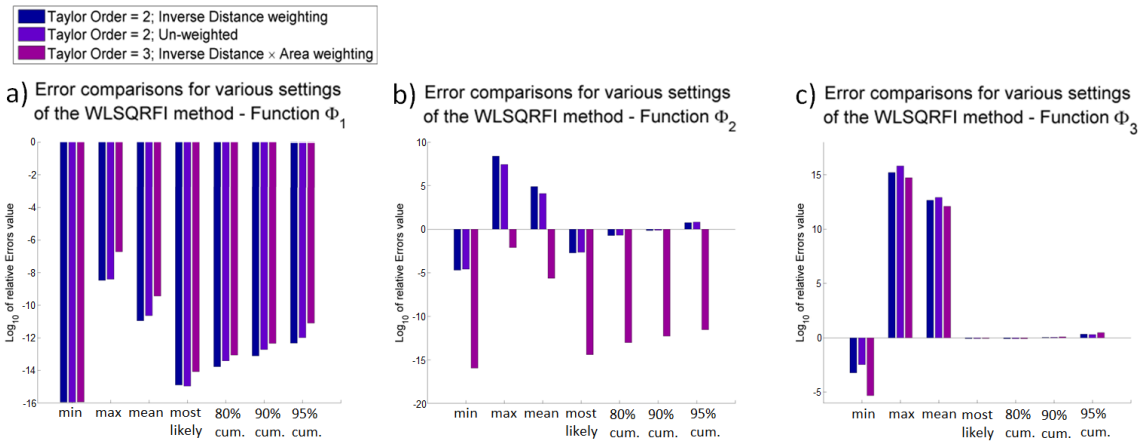

Figure 12. Comparison of GR errors for various WLSQR method parameters (Taylor order = 2 & inverse-distance weighting; Taylor order = 2 & unweighted; Taylor order = 3 -16 stencil points- & inverse-distance × area weighting) for a) ϕ_1**; b)** ϕ_2**; c)** ϕ_3

Figure 11 showcases a certain correlation between low geometric quality regions and large errors in gradient reconstruction, specifically in boundary elements (poor skewness and smoothness) and poor aspect ratio elements. In terms of the LSQR method, two aspects become clear: first, selection of the parameters can mean the difference between unacceptable and acceptable errors in the calculation of gradients (as inferred from Fig. 12b)). Second, a good accuracy GR cannot be recovered for certain function-mesh combinations, as shown in Fig. 12c): function ϕ_3 presents relative errors $\gtrsim 1$ because the mesh does not provide enough *resolution* for the LSQR method to correctly obtain the function gradients for the particular wavelength of the function (it is worth noting that a similar issue will arise in a regular structured mesh without sufficient resolution).

We can conclude that a compromise must be made between the Taylor series order (which determines the number of stencil points), the resolution of the mesh and our previous knowledge of the behavior of functions and variables in the domain in order to ensure good accuracy in the gradient reconstruction.

V. MFAM Benchmark results for the anisotropic diffusion problem

One of the main arguments against the use of MFAMs is that the numerical errors due to lack of mesh "regularity" are, potentially, of the same order than those caused by numerical diffusion in a regular structured mesh. This section presents a "benchmark" simulation to compare these errors: the numerical problem presented in Section II.A may be generalized to take into account a curved magnetic field (variable alignment of the magnetic field directions -variable α- with respect to the cartesian coordinates), so that a comparison between meshes is possible.

In Fig. 13 we compare solutions in both regular and aligned meshes (with the same number of elements) for a magnetic field generated by a current traversing a wire and a simulation domain both arbitrarily large and at an arbitrary distance from the wire; again, the main parameter in the simulation is $\Theta = {}^{D_\parallel}/_{D_\perp} = 10$ and the MFAM simulation is solved with a WLSQ method with Taylor order = 1 (up to the first order cross derivatives) and inverse-distance weighting (which was found to produce the lowest GR errors for this particular case). Figure 14 shows the average density evolution in the initial low density region (pictured at $t' = 0$ in Fig. 13) in both meshes and accounts for the difference between the two solutions due to numerical errors.

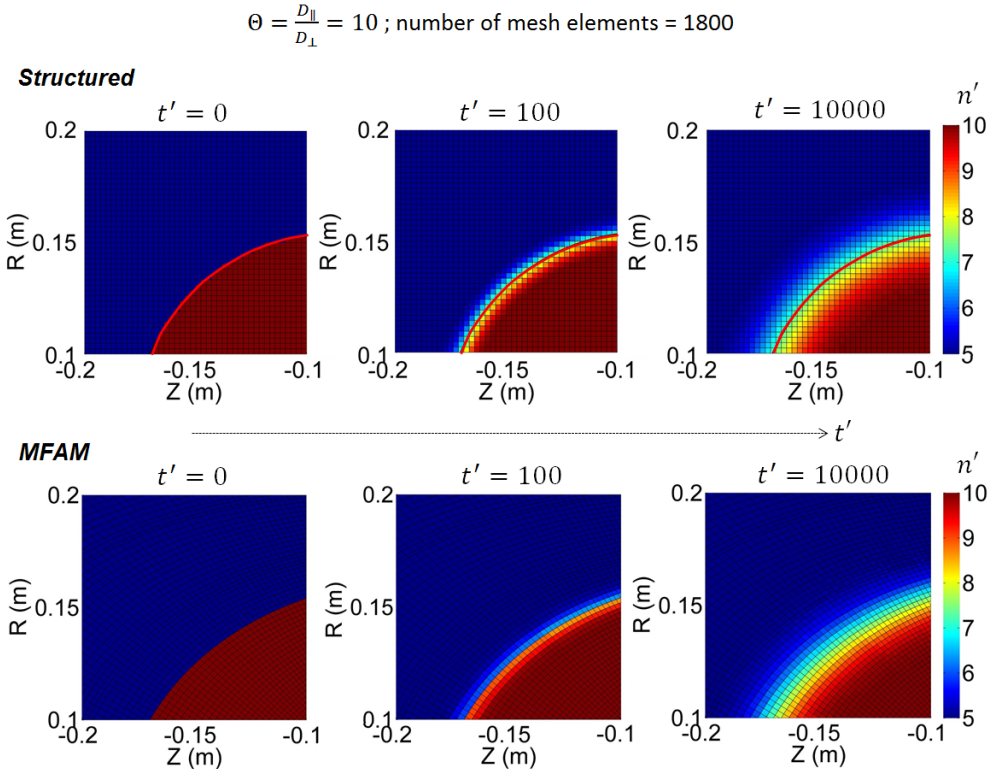

Figure 13. Anisotropic diffusion problem solution in structured (top) and MFAM (bottom) meshes

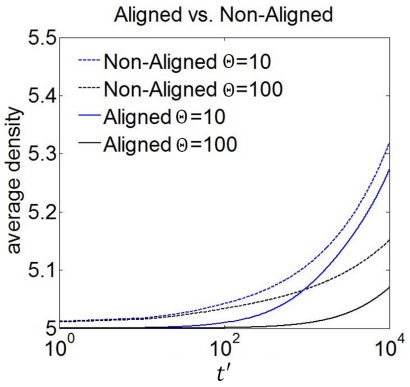

Figure 14. Evolution of average density due to diffusion @ initial "low density" region for Structured and MFAM meshes (different Θ values)

Typical numerical discretization errors appear in MFAM elements due to issues in gradient reconstruction, but not due to numerical diffusion. As evidenced by the results, these errors are small in comparison to global errors caused by numerical diffusion in the structured mesh and imply that both solutions will diverge for sufficiently large times.

Considering that the simulation for the MFAM is solving the *exact* diffusion problem, albeit with the introduction of numerical discretization errors, it is understood that, in general, MFAMs offer a solution which is more consistent with the actual evolution problem than the structured mesh for similar mesh refinement.

An additional discretization error in MFAMs appears because magnetic stream-lines and lines of constant magnetic scalar potential lose their local curvature when mesh elements are generated (Fig. 7), as element facets are always straight. This error is difficult to quantify, although it is presumably small and, formally, does not affect the validity of applying a purely diagonal second order Diffusion term (i.e., no numerical diffusion appears because of it).

VI. Conclusions

The previous sections have shown that large anisotropicities in the diffusion problem are difficult to recover in a regular structured mesh without extensive refinement of the mesh, which would typically involve large computational resources to solve the problem accurately. In MFAMs this problem disappears, by definition, although numerical discretization errors are still present.

For smaller anisotropicity levels, the relatively smaller numerical diffusion errors might be traded-off against the difficulties of using the non-structured mesh: the understanding that gradient reconstruction in a MFAM might cause large errors for certain types of solutions (if the method parameters are incorrectly selected) and the general added difficulty of handling a non-structured problem, purely from a coding perspective.

In this regard, we argue that plasma discharges in electric propulsion devices happen under complex magnetic topologies (with distinct regions of confinement) and depend greatly on the operating parameters of these devices; this means that prior knowledge of the anisotropicity level in the different transport terms of the governing equations is difficult to attain. Consequently, arbitrarily large refinement of a structured mesh might be needed to deal with numerical diffusion. Furthermore, issues in gradient reconstruction may also appear in structured meshes if mesh resolution and the order of the method are not correct; in the case of MFAMs, various strategies have been presented in this work in order to provide additional confidence on our capability to deal with errors introduced by "non-regularity" in the mesh.

Considering all of the above, we conclude that the use of MFAMs for the simulation of magnetically confined discharge plasmas (or specific populations within them), modeled as highly anisotropic fluids, in electric propulsion devices, provides a distinct advantage in bounding numerical errors in the solution, as long as specific challenges in these meshes are taken into account.

Future work will be oriented toward adding "attractor points" in MFAM meshing strategies for additional

control over mesh refinement as well as understanding the possible benefits of mesh quality improvement methods in boundary elements for problems with non-trivial boundary conditions.

Furthermore, the authors are continuing with development on the NOMADS platform; related to numerical simulations, it is expected that the extent of errors caused by lack of mesh regularity in the MFAM may be quantified for plasma discharges in characteristic conditions of electric propulsion devices.

VII. Acknowledgments

This work has been supported by Spain's R&D National Plan, grant number ESP2013-41052-P.

Additionally, the authors would like to acknowledge Samuel Araki and Richard Wirz for their description of the *exponential stretching method* for contour level selection in MFAM meshing, as it consistently provides the best spacing properties amongst the surveyed algorithms.

References

[1]R. Marchanda, M. Dumberrya, "CARRE: a quasi-orthogonal mesh generator for 2D edge plasma modeling", Computer Physics Communications, Volume 96, Issues 2–3, Pages 232–246, August 1996

[2]Ioannis G. Mikellides, Ira Katz, Richard R. Hofer, Dan M. Goebel, Kristi de Grys, and Alex Mathers, "Magnetic shielding of the channel walls in a Hall plasma accelerator", Physics of Plasmas 18, 2011

[3]Anderson, D. V., "Axisymmetric Multi-fluid Simulation of High Beta Plasmas with Anisotropic Transport Using a Moving Flux Coordinate Grid," Journal of Computational Physics, Vol. 17, pp. 246-275, 1975.

[4]Meier, E. T., Lukin, V. S., and Shumlak, U., "Spectral Element Spatial Discretization Error in Solving Highly Anisotropic Heat Conduction Equation," Computer Physics Communications, Vol. 181, pp. 837-841, 2010.

[5]Samuel J. Araki, Richard E. Wirz, "Magnetic Field Aligned Mesh for Ring-Cusp Discharge Chambers", 50th AIAA/ASME/SAE/ASEE Joint Propulsion Conference, July 2014

[6]Diego Escobar and Eduardo Ahedo, "Two-Dimensional Electron Model for a Hybrid Code of a Two-Stage Hall Thruster", IEEE Transactions on Plasma Science, Vol. 36, No. 5, October 2008

[7]Albert Simon, "Diffusion of Arc Plasmas across a Magnetic Field", 2nd Geneva Conference on Peaceful Uses of Atomic Energy, Vol. 32 p. 366, Geneva, 1959

[8]Wirz, R. E., "Discharge Plasma Processes of Ring-Cusp Ion Thrusters", Ph.D. thesis, California Institute of Technology, Pasadena, California, 2005.

[9]Boris Diskin, James L. Thomas, "Effects of mesh regularity on accuracy of finite-volume schemes", 50th AIAA Aerospace Sciences Meeting including the New Horizons Forum and Aerospace Exposition, January 2012, AIAA 2012-0609

[10]Emre Sozer, Christoph Brehm and Cetin C. Kiris, "Gradient Calculation Methods on Arbitrary Polyhedral Unstructured Meshes for Cell-Centered CFD Solvers", 52nd Aerospace Sciences Meeting, 2014

Bibliography

[1] Diego Escobar Anton. Motores de efecto hall de alto impulso específico. 2005.

[2] Daniel G Courtney and Manuel Martinez-Sanchez. Diverging cusped-field hall thruster (dcht). In *Proc. 30th Int. Electric Propulsion Conf.(Florence, Italy)*, 2007.

[3] Samuel J Araki and Richard E Wirz. Automatic magnetic field aligned mesh generation for a ring-cusp discharge chamber.

[4] Roger M Myers, Maris A Mantenieks, and Michael R LaPointe. *MPD thruster technology*. National Aeronautics and Space Administration, 1991.

[5] Eduardo Ahedo. Plasmas for space propulsion. *Plasma Physics and Controlled Fusion*, 53(12):124037, 2011.

[6] Dan M Goebel and Ira Katz. *Fundamentals of electric propulsion: ion and Hall thrusters*, volume 1. John Wiley & Sons, 2008.

[7] Sarah Stansbury. Low thrust transfer to GEO: Comparison of Electric and Chemical propulsion.

[8] Edgar Y Choueiri. New dawn for electric rockets. *Scientific American*, 300(2):58–65, 2009.

[9] David Manzella. Low cost electric propulsion thruster for deep space robotic missions. In *2007 NASA Science Technology Conference, University of Maryland, MD*, volume 7, 2007.

[10] Alex Kieckhafer and Lyon B King. Energetics of propellant options for high-power hall thrusters. *Journal of propulsion and power*, 23(1):21–26, 2007.

[11] K Matyash, R Schneider, A Mutzke, O Kalentev, F Taccogna, N Koch, and M Schirra. Comparison of spt and hemp thruster concepts from kinetic simulations. 2009.

[12] Mario Merino Martínez. *Analysis of Magnetic Nozzles For Space Plasma Thrusters= Análisis de Toberas Magnéticas para Motores Espaciales de Plasma*. PhD thesis, Aeronauticos, 2013.

[13] M Merino-Martınez. 2d plasma flow in a magnetic nozzle with a bi-modal electron energy distribution function. 2012.

[14] Benjamin W Longmier, Leonard D Cassady, Maxwell G Ballenger, Mark D Carter, Franklin R Chang-Díaz, Tim W Glover, Andrew V Ilin, Greg E McCaskill, Chris S Olsen, Jared P Squire, et al. Vx-200 magnetoplasma thruster performance results exceeding fifty-percent thruster efficiency. *Journal of Propulsion and Power*, 27(4):915–920, 2011.

[15] John Blandino, Nikolaos Gatsonis, Mark Cappelli, Alec Gallimore, Iain Boyd, Rodney Burton, Manuel Martinez-Sanchez, Oleg Batischev, John Williams, Azer P Yalin, et al. Overview of electric propulsion research in us academia. In *39th AIAA/ASME/SAE/ASEE Joint Propulsion Conference and Exhibit*, pages 20–23, 2003.

[16] European Commission. CORDIS: In-Space electrical propulsion and station keeping. http://cordis.europa.eu/programme/rcn/664648_en.html, 2014. [Online; accessed 2015-05-16].

[17] Richard R Hofer, Peter Y Peterson, Alec D Gallimore, and Robert S Jankovsky. A high specific impulse two-stage hall thruster with plasma lens focusing. In *27th International Electric Propulsion Conference, Pasadena, CA*, 2001.

[18] GJM Hagelaar. Modelling electron transport in magnetized low-temperature discharge plasmas. *Plasma Sources Science and Technology*, 16(1):S57, 2007.

[19] Robert J Goldston and Paul Harding Rutherford. *Introduction to plasma physics*. CRC Press, 1995.

[20] Albert Simon. Diffusion of arc plasmas across a magnetic field. *Journal of Nuclear Energy (1954)*, 7(3-4):278–278, 1958.

[21] Richard E Wirz. *Discharge plasma processes of ring-cusp ion thrusters*. PhD thesis, California Institute of Technology, 2005.

[22] Qinghai Zhang, Hans Johansen, and Phillip Colella. A fourth-order accurate finite-volume method with structured adaptive mesh refinement for solving the advection-diffusion equation. *SIAM Journal on Scientific Computing*, 34(2):B179–B201, 2012.

[23] Nicolas Crouseilles, Matthieu Kuhn, and Guillaume Latu. Comparison of numerical solvers for anisotropic diffusion equations arising in plasma physics. 2014.

[24] Emre Sozer, Christoph Brehm, and Cetin C Kiris. Gradient calculation methods on arbitrary polyhedral unstructured meshes for cell-centered cfd solvers. 2014.

[25] David V Anderson. Axisymmetric multifluid simulation of high beta plasmas with anisotropic transport using a moving flux coordinate grid. *Journal of Computational Physics*, 17(3):246–275, 1975.

[26] ET Meier, VS Lukin, and Uri Shumlak. Spectral element spatial discretization error in solving highly anisotropic heat conduction equation. *Computer Physics Communications*, 181(5):837–841, 2010.